ISSN 0140-3818
SSSU Report No. 20

UNIVERSITY OF SOUTHAMPTON

DEPARTMENT OF SHIP SCIENCE

FACULTY OF ENGINEERING AND APPLIED SCIENCE

A MODIFIED LIFTING LINE ANALYSIS FOR SEMI-BALANCED SHIP SKEG-RUDDERS

By A.F. Molland, Ph.D.

April 1985

Ship Science Report No. 20

A MODIFIED LIFTING LINE ANALYSIS FOR SEMI-BALANCED SHIP SKEG-RUDDERS

A.F. MOLLAND

1985

Ship Science Report No. 20

SUMMARY

A modified lifting line theory is developed which supports the form of skeg-rudder experimental free-stream data obtained previously, and forming the subject of separate reports.

It is demonstrated that satisfactory predictions of the form of the spanwise loadings for different skeg and rudder angles can be made using lifting line theory with the effect of the skeg being incorporated as local incidence reduction and the effects of the mid-span and tip trailing vortices being incorporated as twist corrections to the local incidence. The correct magnitude of the distributions is obtained by applying suitable empirical corrections. Chordwise centre of pressure is derived empirically.

It is concluded that whilst the theoretical approach is relatively simple and requires empirical correction, it gives very realistic predictions of skeg-rudder performance characteristics.

The theory is used to provide a limited extension to the experimental data. Predictions using the modified theory show that, for fixed aspect ratio and taper ratio, changes in the skeg depth have the largest influence on the production of lift whereas changes in the skeg chord and sweep mainly affect the stock position and the required balance area.

CONTENTS PAGE

1. INTRODUCTION

Extensive experimental results of tests to determine the free-stream characteristics of semi-balanced ship skeg-rudders are reported in Refs.1, 2, 3 and 4.

A theory has been developed (Ref.5) to provide some theoretical evidence for the form of the experimental data, and to allow an extension of the experimental results.

In the theoretical analysis, lifting line theory, modified to include the specific features of the skeg rudder and to account for the differences between theory and experiment, is used to predict the spanwise load distributions. Chordwise centre of pressure is derived from the application, across the span, of local centres of pressure from section and experimental data.

Sections 2 - 13 of this report describe the development of the basic theory, its modifications and empirical corrections.

Section 14 describes the use of the modified theory and empirical relationships to carry out a small parametric study in which variations in aspect ratio and skeg size are investigated.

2. ANALYSIS METHOD

Ship rudders may be considered as lifting surfaces of relatively low aspect ratio with applications lying mainly in the effective aspect ratio range of 3 to 4.

Such a relatively low aspect ratio range poses problems in respect of the choice of a suitable type of theory; for example, Robinson and Laurmann (Ref.6) describe various theories and conclude that experience has shown that lifting line theory remains applicable for aspect ratios as low as 4, whilst very low aspect ratio theory, such as that due to Jones, provides acceptable results for wings whose aspect ratio does not exceed 1.5. For the aspect ratio range lying between these two theories vortex lattice lifting surface theory would be expected to yield more realistic results for all-movable control surfaces.

However, the experimental data obtained for skeg rudders with square tips have indicated particular physical properties which need to be incorporated in any theoretical analysis. These amount to early separation aft of the skeg (which is influenced by gap flow), a strong tip vortex (which has a marked influence on the spanwise distribution of load near the tip), and a vortex at the break between the skeg and all-movable parts.

Whilst lifting surface theory has the advantage of providing chordwise as well as spanwise loadings and hence centres of pressure, and has been successfully applied to rudders with relatively small (and unstalled) flaps, the theory would require extensive modifications to incorporate the particular physical features exhibited by the skeg rudder. On the other hand simple lifting line theory lends itself better to the incorporation of the skeg rudder features, and is more amenable to empirical corrections, although it should be borne in mind that the theory would be applied at or just below its generally accepted lower aspect ratio limit.

Taking into account the limitations of the various theories, the overall physical characteristics of the skeg rudder, and the fact that the primary objectives of a theoretical analysis were to support and extend the earlier experimental work, it was decided to pursue a lifting line analysis incorporating empirical modifications as necessary.

The overall approach, therefore, has been to determine the spanwise load distributions from a modified lifting line analysis and to apply, across the span, local chordwise centres of pressure from section and experimental data. The analysis for total $CP\bar{c}$ was limited to the movable rudder alone, as this value is the one which is of principal interest in respect of rudder torques; the integration for total values, therefore, required estimates of the proportion of the total chord load carried by the movable (flap) part aft of the skeg, together with the chordwise centre of pressure in way of skeg for the movable (flap) part.

3. OUTLINE OF THE LIFTING LINE ANALYSIS

General :

The method used for deriving the basic spanwise load distribution is generally along the lines of that due to Glauert (Ref.7). In the present analysis the skeg rudder is considered as a special case of a twisted aerofoil. In this case Glauert shows theoretically that the lift curve slope is independent of the twist. Ideally, therefore, it would be assumed that the effect of the skeg would be to change the angle of incidence (measured from the no-lift angle) and to leave the slope of the lift curve unaltered. From the results given in Fig. 1 , where the experimental data from Refs. 1 and 2 have been re-plotted for constant values of δ, these assumptions are seen to be acceptable for small angles and where no separation occurs aft of the skeg. Fig. 1 also indicates that it is not unreasonable to take a similar approach for the α range where early separation aft of the skeg has occurred although, in this case, some (constant) modification to the lift curve slope has taken place and requires incorporation in the analysis.

The rudder geometry used in the analysis is given in Fig. 2 . The effect of the reflection plane is represented by an image rudder and vortex system. The rudder is assumed to have a total span, including its image, of 2S and a taper ratio $(C_T/C_R) = T$.

The rudder is considered as being replaced by a lifting line of length 2S. The co-ordinate y is replaced by the angle θ defined as :

$$y = -S.\cos\theta$$

let $k = 1-T$, or $T = 1-k$, (hence $C_T = C_R(1-k)$)

Area $A_E = (2-k).S.C_R$

and Aspect Ratio $AR = \dfrac{4S^2}{A_E} = \dfrac{4S}{(2-k)C_R}$

At any point on the rudder, $c = C_R(1-k\cos\theta)$ and, at any point, the incidence of the skeg rudder, considered as a lifting line will be :

$$\bar{\alpha} = \alpha - \gamma \qquad \ldots(1)$$

where α = incidence of the movable rudder part

γ = decrease in incidence over the skeg part, at some rudder angle α, to produce the same all-movable value, as shown in Fig.3

i.e. $\bar{\alpha} = \alpha - f(\theta).\gamma(\delta,\alpha)$

where $f(\theta) = 0$ from $\theta = 0$ to $\theta = \varphi$

$= 1$ from $\theta = \varphi$ to $\theta = \pi/2$

and $\gamma(\delta,\alpha)$ can be derived from theoretical and experimental data with no separation on the flap and from experimental data when gap flow and separation are present.

The derivation and use of suitable values of γ is discussed in Section 5.

The circulation Γ at a point θ on the rudder may be expressed as a Fourier series :

$$\Gamma = 4S\ V\ \Sigma\ An\ \sin n\theta \qquad \ldots(2)$$

and since the planform is symmetrical about the mid point $(\pi/2)$, only odd values of n will occur in the series.

The induced velocity ω at a point θ is given (Ref. 7) by :

$$\omega = \frac{V\ \Sigma\ n\ An\ \sin n\theta}{\sin\theta} \qquad \ldots(3)$$

The section experiences a lift force corresponding to two-dimensional motion at the effective angle of incidence $(\bar{\alpha} - \omega/V)$ where ω/V is the induced downwash angle.

$$\text{Local lift coefficient } C_L = m(\bar{\alpha} - \omega/V) \qquad \ldots(4)$$

where m is the two-dimensional lift curve slope, allowing for thickness and viscosity effects.

Hence at any point $\Gamma = \frac{L}{\rho V}$

$$= \frac{C_{L}.c.V}{2}$$

$$= \frac{m}{2}.c.V(\bar{\alpha} - \omega/V) \qquad \ldots(5)$$

Incorporating the value of induced velocity from equation (3)

$$\Gamma = \frac{m}{2}.c.V(\bar{\alpha} - \frac{\Sigma n\ An \sin n\theta}{\sin\theta}) \qquad \ldots(6)$$

equating (2) and (6)

$$4S\ V\ \Sigma\ An \sin n\theta = \frac{m}{2}.c.V(\bar{\alpha} - \frac{\Sigma n\ An \sin n\theta}{\sin\theta})$$

$$\Sigma An \sin n\theta = \frac{m\ C_{R}(1-k\cos\theta)}{8S}\ (\bar{\alpha} - \frac{\Sigma n\ An \sin n\theta}{\sin\theta})$$

$$\frac{\Sigma An \sin n\theta}{(1-k\cos\theta)} = \mu\bar{\alpha} - \frac{\mu \Sigma n\ An \sin n\theta}{\sin\theta}$$

where $\mu = \frac{m\ C_{R}}{8S}$

$$\therefore\ \Sigma An \sin n\theta.\ \frac{\sin\theta}{1-k\cos\theta} + \mu \Sigma n\ An \sin n\theta = \mu\bar{\alpha}\sin\theta$$

$$\text{or}\quad \Sigma\left[An \sin n\theta(\mu n + \frac{\sin\theta}{1-k\cos\theta})\right] = \mu.\bar{\alpha}.\ \sin\theta \qquad \ldots(7)$$

This fundamental equation must be satisfied at all points on the rudder between 0 and $\pi/2$. From the form of this equation and $\bar{\alpha} = \alpha - \gamma$ it is possible to separate the contributions of the all-movable and skeg parts in the form :

$$An(\bar{\alpha}) = \left[a_{n}(\alpha) - b_{n}(\gamma)\right] \qquad \ldots(8)$$

Local lift $L = \rho V \Gamma = \rho V[4S\ V\ \Sigma\ An \sin n\theta]$

$$= 4\ \rho\ S\ V^{2}\ [\Sigma An \sin n\theta]$$

hence the local lift coefficient $C_L = L/\frac{1}{2}\rho c V^2$

$$= \frac{8S}{c} \Sigma An \sin n\theta$$

$$= \frac{8S}{C_R(1-k.\cos\theta)} \Sigma(a_n(\alpha) - b_n(\gamma)) \sin n\theta \qquad ...(9)$$

(also, overall $C_L = \pi AR(a_1(\alpha) - b_1(\gamma))$ although in the analysis, overall C_L is derived from a spanwise integration of local C_L)

and local induced drag coefficient $C_{Di} = C_L.\frac{\omega}{V}$ ...(10)

Number of Control Points (n) chosen along Rudder :

The fundamental equation (7) has to be satisfied at all points along the rudder. A large number of control points is desirable since the analysis has to include the facility to vary $\bar{\alpha}$ along the rudder (with a discontinuity at the end of the skeg), and to superimpose vortices at the tip and at the break between skeg and all-movable parts (see later). Several values of n were tested for the various required values of aspect and taper ratio. In order to obtain a suitable spacing of stations near mid span (in order that different skeg depths could be investigated) n was chosen as 20.

The spacing near mid span allowed skeg depth/span ratios of 0.36, 0.43, 0.50, 0.57 and 0.63 to be investigated (Fig.4). This approach does not, of course, represent a discontinuity of incidence at the skeg to all-movable break but corresponds to a continuous change of incidence over a small region of the order of 6% to $7\frac{1}{2}$% of span.

4 MODIFICATIONS AND ADDITIONS TO THE BASIC LIFTING LINE THEORY

Modifications and additions to the basic theory are required due to the particular physical properties of the skeg rudders being modelled, as mentioned earlier. These entail incorporating downwash contributions from the superimposed tip and mid-span trailing vortices and any empirical corrections necessary to take account of the differences between theoretical lift curve slopes and those derived from experiment.

4.1 Vortex Model

The idealised vortex model assumed for the analysis is shown in Fig. 5 and comprises :

(a) A basic trailing vortex sheet due to the lifting line.

(b) A superimposed trailing tip vortex with a solid core, whose strength is assumed to be a function of α, T and AR.

(c) A superimposed trailing vortex, with a solid core, at the break between the skeg and all-movable parts, whose strength is assumed to be a function of α and δ.

The bound vorticity associated with (b) and (c) is assumed to be concentrated on the lifting line. Further comments on assumptions (b) and (c) are given later in Section 6.

The general forms of the expected distributions of downwash due to these three component parts are shown diagrammatically in Fig. 6.

4.2 Incorporation of Superimposed Vortices in the Analysis

Lifting line theory requires that at any section, equation (4)

$$C_L = m(\bar{\alpha} - \omega/V)$$
$$= m(\bar{\alpha} - \alpha_i)$$

where α_i is the downwash angle due to the vortex sheet.

It is initially assumed that the influence of the additional trailing vortices is to superimpose a downwash or upwash α_T on that due to the vortex sheet. e.g. when the local modification α_T leads to an increase in C_L :

$$C_L = m(\bar{\alpha} - (\alpha_i - \alpha_T)) \qquad ...(11)$$
$$= m(\bar{\alpha} - \alpha_{i1}) \qquad ...(12)$$

where $\alpha_{i1} = \alpha_i - \alpha_T$ and represents the net downwash including the effect of the superimposed vortices.

Since the correction α_T cannot be retained directly as a downwash correction in the lifting line equations, equation (11) is re-written in the form :

$$C_L = m(\bar{\alpha} + \alpha_T) - \alpha_i) \qquad ...(13)$$

and for the solution of the fundamental equation (7) the correction is treated, in effect, as equivalent local twist α_T applied to the local angle of attack. The values derived for $\alpha_T(\theta)$ for the two vortices, and used in the analysis, are given in Section 6.

4.3 Corrections to Theoretical Lift and Drag Values

As would be expected for relatively low aspect ratios, the lifting line analysis results in lift curve slopes in excess of experimentally derived values. The basic analysis, in effect, derives what may be assumed to be a 'mean' induced downwash in the neighbourhood of the rudder, and neglects any change in downwash along the chord. Also, the flow is in all places assumed parallel to the X-Axis, whereas cross flow will occur near areas of rapid pressure change, such as near the tip. These influences become more important with increase in chord relative to span

(i.e. decrease in AR). In the present analysis it is assumed that the flow remains parallel to the X-Axis and that the required decrease in C_L predicted by the lifting line analysis is caused by an increase in the 'mean' downwash.

Basic lift curve slopes for the all-movable case were derived from the lifting line analysis for taper ratios of 0.60, 0.80 and 1.0 and aspect ratios 2, 3 and 4. Equivalent all-movable slopes were derived from published experimental data, and the results for the 'gaps open' case of the present work.

This leads to a correction to the lifting line result of the form :

$$C_{Lc} = C_{Lt} \cdot a(AR) \qquad \ldots(14)$$

where C_{Lt} is the theoretical lift coefficient from lifting line theory

C_{Lc} is the corrected lift coefficient.

a is the ratio of the experimental to the theoretical and is a function of aspect ratio.

It is assumed that the form of the spanwise distribution of lift remains the same but that its magnitude across the span is reduced by the factor a. Although this approach is approximate, comparisons with the experimental results of Ref. 8 for the all-movable case of AR = 3.4, for example, indicate that lifting line predictions modified by this method lead to spanwise distributions which are very satisfactory for the purposes of the present investigation. The values derived for factor a, and used in the analysis, are given in Section 7.

Correction to Downwash :

Assuming that the decrease in theoretical C_L is caused by an increase in 'mean' downwash, and the general form of equations (4) and (12) are preserved, then equation (12) can be written as :

$$C_{Lc} = m(\bar{\alpha} - \alpha_{i2}) \qquad \ldots(15)$$

and $$\alpha_{i2} = \bar{\alpha} - C_{Lc}/m \qquad \ldots(16)$$

where α_{i2} is the final net downwash including the effects of the superimposed vortices and the empirical correction to lift.

α_{i2} is used to compute the induced drag, and the local induced drag coefficient can now be written as :

$$C_{Di} = C_{Lc} \cdot \alpha_{i2} \qquad \ldots(17)$$

Values for the profile drag coefficient C_{Dp} for the flapped (skeg) and all-movable parts may be derived from suitable experimental data, hence the local drag coefficient C_D may be derived as :

$$C_D = C_{Dp} + C_{Di} \qquad \ldots(18)$$

and local normal force coefficient :

$$C_N = C_{Lc}\cos\alpha + C_D\sin\alpha \qquad \ldots(19)$$

The local normal force coefficients are used in the subsequent derivation of the chordwise and spanwise centres of pressure. An outline of the derivation of suitable values for C_{Dp} is given in Section 8.

5. DERIVATION OF SKEG INCIDENCE REDUCTION, γ

Suitable γ values for Rudder No.1 were derived for each rudder and skeg angle, by adjusting γ in the modified lifting line analysis until satisfactory

agreement with the spanwise distribution derived from the pressure measurements was achieved. Rudder No.1 had an average effective flap ratio of 0.70.

The γ values so obtained are shown in Fig.10, and suitable equations representing these results are :

up to separation aft of the skeg :

$$\gamma = 0.23\delta \qquad \ldots(20)$$

after separation :

$$\gamma = 0.3\alpha - 3 + 0.39\delta \qquad \ldots(21)$$

In order to confirm these values, and to provide more general data for different flap sizes, the derivation of γ values from alternative sources was investigated.

Considering, firstly, angles up to the onset of flap separation the theoretical results of Ref.9 were investigated and suitably adapted; in this reference Glauert applies thin aerofoil theory to a two-dimensional flapped foil.

In the notation of the present work

$$C_L = \left[\frac{\partial C_L}{\partial \beta}.\beta + \frac{\partial C_L}{\partial \delta}.\delta\right]$$

$$= \left[\frac{\partial C_L}{\partial \beta}(\alpha - \delta) + \frac{\partial C_L}{\partial \delta}.\delta\right] \qquad \ldots(22)$$

Since, in the unseparated range, lines of constant δ to a base of α will be parallel and γ will be independent of α, γ can be obtained direct from the result at $C_L = 0$. Hence replacing α by γ at $C_L = 0$

$$\frac{\partial C_L}{\partial \beta}(\gamma - \delta) = -\frac{\partial C_L}{\partial \delta}.\delta$$

and $$\gamma = \delta\left(1 - \frac{\partial \beta}{\partial \delta}\right) \qquad \ldots(23)$$

where $\frac{\partial \beta}{\partial \delta}$ is commonly termed the flap effectiveness ratio.

Glauert derived the theoretical expression

$$\frac{\partial \beta}{\partial \delta} = 1 - \frac{2}{\pi}\cos^{-1}\sqrt{\frac{c_f}{c}} + \frac{2}{\pi}\sqrt{\frac{c_f}{c}\left(1 - \frac{c_f}{c}\right)}$$

$$= \frac{2}{\pi}\left[\sqrt{\frac{c_f}{c}\left(1 - \frac{c_f}{c}\right)} + \sin^{-1}\sqrt{\frac{c_f}{c}}\right] \qquad \ldots(24)$$

Due to viscous effects and section thickness, experimental values will be smaller than theoretical values. Much data is brought together (including Refs. 12 and 13) in Ref. 10 to demonstrate this.

A mean line of $\gamma = 0.23\delta$, equation (20), satisfactorily represents the correlation between the lifting line analysis and the pressure measurements of the present work. The effective flap ratio $\frac{c_f}{c}$ of Rudder No. 1 is 0.7 and, based on this, the Glauert theoretical result requires modification to :

$$\frac{\partial \beta}{\partial \delta} = \frac{2}{\pi}\left[0.48\sqrt{\frac{c_f}{c}\left(1 - \frac{c_f}{c}\right)} + \sin^{-1}\sqrt{\frac{c_f}{c}}\right] \qquad \ldots(25)$$

This represents a decrease in the theoretical effectiveness ratio of approximately 15%.

The relationship for γ (for angles up to the onset of separation) thus becomes:

$$\gamma = \delta\left[1 - \frac{2}{\pi}\left(0.48\sqrt{\frac{c_f}{c}\left(1 - \frac{c_f}{c}\right)} + \sin^{-1}\sqrt{\frac{c_f}{c}}\right)\right] \qquad \ldots(26)$$

This result allows the influence of flap chord size to be incorporated in the analysis.

It can be noted that this change in γ with change in flap size is supported by the trend of the results from Refs. 12 and 13 shown in Fig. 7 and discussed later. Thin aerofoil theory suggests that the flap effectiveness ratio should be independent of aspect ratio. Experimental and theoretical results reproduced in Ref. 10 confirm that only very small variations occur for aspect ratios down to about 2. Consequently, up to the onset of separation, it is assumed that γ is independent of aspect ratio and that

equation (26) is suitable for the aspect ratio range considered in the present investigation.

Extensive published experimental data are available for small flaps and flap angles. The need for data for large flap sizes (60% - 75% chord) and large flap deflections (up to 35° leading to separation on the flap) severely limited the published data suitable for the present investigation.

Detailed experimental measurements are, however, available from Refs.11, 12 and 13 for flap sizes of 30%, 50% and 80% chord, and these were used to assess γ values up to and after the onset of separation on the flap. The results are for flapped foils with sealed gaps in two-dimensional flow. Such foils do display separation aft of the hinge and discontinuities in their lift curves, as is shown in Fig. 7 although its onset occurs at higher δ angles than with gaps open.

C_N curves for constant δ to a base of α derived from Refs.12 and 13 are shown in Fig. 8 (for clarity, the results for the 30% flap have been omitted from the graph). Values of γ obtained from this graph are shown in Fig.10. Because there is a small decrease in the normal force curve slope after separation has occurred (compared with the all-movable case, as is seen in Fig.8) the γ values after separation show some dependence on α, as is demonstrated in Fig. 10. Up to the onset of separation the γ values are independent of α, as would be expected.

It should be noted that only normal force coefficients (C_N) were presented in these reports, drag not having been measured. Approximate estimates of C_L were made allowing for a profile drag coefficient of 0.02 for the all-movable case ($\delta = 0$) and up to 0.07 with separation on the flap at large angles of attack. These estimates indicated negligible change in γ up to $\alpha = 20^{\circ}$ and up to $\frac{1}{2}^{\circ}$ increase in γ at $\alpha = 30^{\circ}$.

The γ values derived from Refs.12 and 13 show

very similar trends to those derived by correlation of the lifting line theory with the pressure measurements, although after separation they are up to 1° lower. The experimental values are for sealed gaps and for a more realistic comparison some assessment of the influence of open gaps is required. Several papers report ad hoc tests on the effects of gaps, but only Ref.14 could be found which investigated systematically the influence of gap size for a plain flap. Whilst the flap was only 30% chord the data do offer some guidance on these effects. Gap influence on γ is shown in Fig.9 and it is seen that with open gaps, and with separation on the flap the normal force is decreased and γ is increased by between 1° and $1\frac{1}{2}^{\circ}$, the smaller changes in γ occurring at the larger α values.

It would, therefore, be expected that the effect of gaps, and the effect of the $C_N \sim \alpha$ presentation discussed earlier, would be to raise the results of the gap closed data in Fig.10 to a little above the pressure correlated results as given by equation (21). The final slopes of the corrected data sets will also be close to that contained in equation (21). It is considered that the foregoing reasoning justifies the basis of equation (21) and the order of magnitude of the values obtained.

Ref.14 indicates that up to separation the influence of the gap is relatively small and in the context of the present discussion can be neglected.

Figs.7 and 8 also illustrate the order of difference in normal force and hence γ between the 50% and 80% flap cases. Before separation the normal force produced by the 80% case is larger than the 50% case; this results in γ increasing with decrease in flap ratio which is also supported by the results of modified thin aerofoil theory, equation (26). After separation the normal force produced by the 80% case falls below the 50% case until, at a higher angle of attack, it becomes larger again. Hence over most of the separated working range γ is larger for the 80% case, i.e. the opposite effect to pre-separation with γ now

increasing with increase in flap ratio. (It should be noted that this reversal of the normal force curves occurs only in the 50% - 80% flap range, the 30% flap case being significantly lower than either of these curves, as shown in Fig.7).

For structural and balance reasons, realistic skeg rudders are unlikely to have an effective C_f/c outside the range 0.60 to 0.75. Over this range the change in γ is no more than 0.5° and is, therefore, small relative to the total γ values for the flap separated conditions. However, for completeness, and to obtain the relative effects of change in flap size, an approximate correction is applied to equation (21) to reflect this effect. The proposed correction is $+0.4(\frac{C}{c}f - 0.7)(28 - \delta)$ which tends to zero as $C_f/c \to 0.7$ and the sign of the correction changes at $\delta = 28^\circ$ which is the approximate angle at which the normal force curve for the 80% flap again crosses the 50% flap curve (as shown in Fig. 7). The effect of this correction on the basic $C_f/c = 0.7$ line is illustrated (for $\alpha = 30^\circ$) in Fig. 10.

Thus, after the onset of separation the value of γ used in the analysis is expressed as follows :

$$\gamma = (0.3\alpha - 3 + 0.39\delta) + 0.4\ (\frac{C}{c}f - 0.7)\ (28 - \delta) \qquad ...(27)$$

No data could be found, for large flap sizes, to determine the influence of aspect ratio on γ in the separated condition. As already discussed, γ is independent of aspect ratio pre-separation and it is also assumed that this is the case after separation. It should be added that if the curves of C_N for constant δ in Fig.8 are decreased due to aspect ratio, and it is assumed that the decrease is in the same proportion as that for the all-movable ($\delta = 0$) case (which would not seem unreasonable), then γ for the separated cases also would remain unchanged for changes in aspect ratio. After the onset of separation, therefore, it is assumed that γ is independent of aspect ratio and that equation (27) is suitable for the relatively limited aspect

ratio range considered in the present investigation.

In Section 9 it is determined that the onset of separation can be satisfactorily represented by equation (37) :

$$\alpha_{sep} = 4 + 0.4(\beta + 15)$$

6. ASSUMPTIONS FOR THE DOWNWASH INDUCED BY THE SUPERIMPOSED VORTICES

6.1 General

In order to provide general guidance on the form of the downwash modifications, and hence the equivalent twist to be applied to the lifting line equations, the superimposed vortex systems are assumed to be idealised as single trailing vortices with solid cores. An outline of the assumptions made leading up to this idealisation is given.

At the rudder tip a vertical vortex sheet is generated which increases in length with increase in incidence. The development of such a sheet has been described, for example, by Küchemann, Ref. 15. The tip vortex sheet might be expected, and is hence assumed, to roll up into a conical vortex, which in turn is assumed to be replaced by a concentrated 'vortex' (which increases in strength downstream from its apex). Such a replacement has, for example, been made by Cheng, Ref. 16, and others, in the development of delta wing theory. Cheng points out that this solution also exhibits certain general characteristics of edge separation observed at low speed for low AR aerofoils.

The mid vortex is initiated as a vertical vortex sheet springing from the abrupt discontinuity between the skeg and all-movable parts near the leading edge; this may be considered as a 'part-span vortex' in the terminology

of Ref.15 and thought of as a continuation of the bound vortices which do not travel outboard. The mid vortex is also assumed to roll up and be replaced by a concentrated conical vortex.

In the analysis, each vortex is then considered as being represented by a single trailing vortex of constant 'mean' strength in the neighbourhood of the rudder. Thus the downwash induced by each trailing vortex is initially assumed to have the general form of the normal velocity distribution for a vortex with a solid core. The strength of the tip vortex is assumed to be a function of incidence, tip chord (hence taper ratio) and aspect ratio, whilst that of the mid-vortex is assumed to be a function of incidence.

The spanwise pressure distributions are used to locate the position of the vortices and their approximate 'mean' core sizes, and no attempt is made to theoretically predict these properties. The actual downwash distributions were obtained by suitably adjusting the superimposed twist in the basic analysis until the form of the distribution of load agreed with the experimental results.

6.2 Tip Trailing Vortex

The induced downwash (applied to equation (7) as equivalent twist) is assumed to be of the form :

$$\alpha_{T1} = \int \left[H_1(\theta), \alpha, AR, T \right]$$

where $H_1(\theta)$ is the general form of the variation of downwash across the span at a particular incidence, aspect ratio and taper ratio.

It is assumed that the influence of the tip vortex is responsible for the non-linear component of lift normally exhibited by low aspect ratio lifting surfaces, as was concluded by Küchemann, Refs.15 and 17.

Based on the results in Refs.18, 19 and others, it is reasoned in Ref.17 that the non-linear increment of

lift decreases with increasing aspect ratio and increases with increasing taper ratio, and is approximately a quadratic function of incidence.

The non-linear component has been derived semi-empirically as being a function of α^2 by several investigators, such as Refs.20 and 21. These are generally based on the hypothesis of Betz, Ref.22, in which the non-linear (α^2) component arises from cross flow and is a function of a cross flow drag coefficient; in this approximation the non-linear increment is assumed to be uniformly distributed over the planform. In the present analysis the non-linear component is assumed to be due to the tip vortex, as mentioned earlier.

Ref.20 assumes the non-linear component to be proportional to 1/AR, which tends to zero as AR tends to infinity as is expected experimentally. The procedure adopted in Ref.19 also amounts to an inverse function of AR.

From an investigation of the cross flow drag coefficient values in Ref.20 the non-linear component is found to be proportional to T; this is also implied in Ref.19.

Based on the above comments it would appear reasonable, for the purposes of the present investigation, to assume the tip vortex strength and hence the induced normal velocity to be a function of $(\alpha^2 T/AR)$.

The final distribution of $H_1(\theta)$, following adjustment by trial in order to bring the form of the distribution of load into line with the experimental results, is shown in Fig.11. The downwash distribution is seen to be asymmetrical which may be partly due to the downstream growth of the vortex in the neighbourhood of the rudder, with the outboard side of the vortex being always approximately aligned with the tip. Also, the influence of taper was required to be increased to $T^{1.5}$ in order to reflect the changes derived from the experiments (including the all-movable case). Empirical constants were introduced simply to correlate the magnitude of the load with experiment at the datum angle.

The resulting equation used in the analysis for the downwash induced by the tip vortex is :

$$\alpha_{T1}(\theta) = H_1(\theta)\ \frac{\alpha^2}{10}\cdot\frac{3}{AR}\cdot\frac{T^{1.5}}{0.465}$$

$$= H_1(\theta)\ \frac{\alpha^2\ T^{1.5}}{AR}\cdot 0.645 \qquad \ldots(28)$$

Fig. 11 and equation (28) indicate that the requirements of the method have led to extremely high values of $\alpha_{T1}(\theta)$ at large angles of attack and, consequently, unreal values of required twist near the tip. Thus, although the method of applying the vortex induced downwash angle as twist may be acceptable in providing the correct spanwise load distribution, the 'twist' so required cannot be considered as, or equated to, real or physical twist.

6.3 Mid Span Trailing Vortex

The induced downwash (applied to equation (7) as equivalent twist) is assumed to be of the form :

$$\alpha_{T2} = \int [H_2(\theta), \alpha, \delta]$$

where $H_2(\theta)$ is the general form of the variation of downwash across the span at a particular incidence.

The vortex is fed with fluid over a relatively short distance and its starting point will be approximately fixed. Inspection of the experimental spanwise distributions suggested that the overall vortex effect is approximately proportional to incidence. Since the vortex is generated by flow through the horizontal gap, as well as the basic pressure differential due to the discontinuity between the skeg and all-movable parts, the growth of the vortex strength will be dependent on α as well as the difference in incidence (δ) between the skeg and all-movable parts.

After some initial comparisons with the experimental results it was assumed that the vortex strength and induced normal velocity is a function of $(\alpha^{0.5}.\delta^{0.5})$.

Since the difference between α and δ is the skeg angle β which may be up to, say, 10° it is apparent that changes in the proportion of dependence on α or δ will not have a large effect on the final result; for $\beta = 0^{\circ}$, α will, of course, be equal to δ for all α values.

The final distribution of $H_2(\theta)$, following adjustment by trial in order to bring the form of the distribution of load into line with the experimental results, is shown in Fig.11. The required downwash distribution was found to be approximately symmetrical, but its position set towards the root; this may be due to the spanwise pressure gradient (e.g. see Ref.3)

causing the vortex to be swept into a region of lower pressure as it moves aft across the chord. A constant is introduced to correlate the magnitude of the load with experiment at the datum angle.

The resulting equation used in the analysis for the downwash induced by the mid-span vortex is :

$$\alpha_{T2}(\theta) = H_2(\theta).\alpha^{0.5}.\delta^{0.5}.2 \qquad \ldots(29)$$

7. DERIVATION OF LIFT CURVE SLOPE CORRECTION FACTOR, a :

All-movable lift curve slopes were derived from the lifting line analysis for taper ratios of 0.60, 0.80 and 1.0 and aspect ratios of 2, 3 and 4. A two-dimensional section slope (m) of 5.5 was assumed in the analysis, this being derived from Ref.23 as applicable for a section thickness ratio of 20% with L.E. roughness. The lift curve slope values for taper ratio 0.6 are shown in Fig.12, and these are adequately represented by the equation :

$$\left[\frac{dC_L}{d\alpha}\right]_{\alpha=0} = \frac{2\pi}{57.3(1.14 + 2/AR)} \qquad \ldots(30)$$

This satisfies the conditions that $dC_L/d \to 0$ and 5.5 as $AR \to 0$ and ∞ respectively.

For comparison, the theoretical lift curve slope for elliptical planform is also given in Fig.12.

Lifting line theory predicts a small increase in slope with decrease in taper ratio. Published experimental all-movable data such as that in Ref 20 and for the all-movable rudders in Ref.1 also indicate only small changes in lift curve slope with change in taper, but in the opposite direction to that predicted by lifting line theory. The influence of taper ratio (T) from lifting line theory for the basic all-movable slope was, therefore, removed by a suitable empirical correction of the form $T^{0.1}/0.95$.

A mean curve representing the experimental data with smooth L.E. from Refs 20 & 24 is given in Fig.12. and a suitable fit to this curve is :

$$\left[\frac{dC_L}{d\alpha}\right]_{\alpha=0} = \frac{1.95\pi}{57.3(1 + 3/AR)} \qquad \ldots(31)$$

The equivalent all-movable 'gaps-sealed' case for the present work with aspect ratio 3 and L.E. roughness was tested, resulting in a lift curve slope of 0.048 (Ref.1).

Since the loss in lift curve slope is principally due to the influence of thickness and L.E. roughness on section slope, a suitable relationship can be a modified form of equation (31) resulting in :

$$\left[\frac{dC_L}{d\alpha}\right]_{\alpha=0} = \frac{1.75\pi}{57.3(1 + 3/AR)} \qquad \ldots(32)$$

In this case $dC_L/d\alpha \rightarrow 5.5$ as $AR \rightarrow \infty$

Preliminary use of equation (32) as a correction in the analysis led to insufficient decrease in the theoretical lift values, and it was, therefore, considered necessary to take account of the influence of gaps on the all-movable configuration.

An all-movable 'gaps open' case had been tested (Ref.1) and this led to a further reduction in lift curve slope compared with the 'gaps-sealed' case.

It is likely that this loss is due primarily to the horizontal gap and the gap around the pintle. Since such effects will not directly modify the two-dimensional section slope it is assumed, for the purposes of the analysis, that this loss is in effect accounted for by a further relative increase in downwash. This assumption is in fact not unreasonable when it can be deduced from Ref.1 that the drag of the 'gaps-open' case for α up to about 16° is C_L^2 dependent and the C_D/C_L^2 slope is increased by the AR decrease predicted by the loss in lift curve slope, suggesting that the increase in C_D over the gaps sealed case is mainly induced, and hence downwash dependent. Hence a suitable curve passing through the 'gaps-open' result in Fig.12 was assumed to be :

$$\left[\frac{dC_L}{d\alpha}\right]_{\alpha=0} = \frac{1.75\pi}{57.3(1 + 3.9/AR)} \qquad \ldots(33)$$

This, therefore, assumes these particular losses to be principally aspect ratio dependent over the aspect ratio range considered and retains the condition that $dC_L/d\alpha \rightarrow 5.5$ as $AR \rightarrow \infty$

An alternative approach, for example, would have been to change the numerator in equation (32) to 1.5π. The reasoning leading up to equation (33) would, however, seem to be more plausible, hence that line was adopted. It should also be noted that over the aspect ratio limits (approximately 2 to 4) under consideration the alternative approaches yield very similar net corrections to the theory.

Hence the overall correction to the basic lift curve slope from lifting line theory is assumed to be of the form :

$$a = \frac{T^{0.1}}{0.95} \times \frac{\frac{1.75\pi}{57.3(1 + 3.9/AR)}}{\frac{2\pi}{57.3(1.14 + 2/AR)}}$$

$$= \frac{T^{0.1}}{0.95} \times \frac{0.875\ (1.14 \times AR + 2)}{(AR + 3.9)} \qquad \ldots(34)$$

8. PROFILE DRAG, C_{Dp}

The present investigation required profile drag data for thick sections with a large flap both at low angles of attack and over the flap stalled range of angles. A search of related published papers did not reveal suitable profile drag data which also included the flap stalled condition. The required information was, therefore, extracted from the experimental results of the present work, Refs.1 & 2.

The drag data was, for Rudder No.1, plotted to a base of C_L^2 as shown in Fig.13; the skeg rudder results, of course, represent the drag of a combination of approximately half all-movable and half skeg (or L.E. flap) parts. Similar plots for Rudder Nos.2 and 3 displayed the same general characteristics.

The all-movable data exhibit expected trends, and the profile drag for the all-movable part can be assumed to be represented by the equation

$$C_{Dp} = 0.017 + 0.12\ C_L^5 \qquad \ldots(35)$$

the second term resulting from the development of separation at higher angles of attack.

For small C_L values and all β values C_{Dp} for the skeg plus all-movable combination is seen to be about 0.02, but at the onset of separation aft of the skeg there is a sudden rise to a much higher value. With increasing incidence C_D is, over a short range, again seen to be proportional to C_L^2; thereafter, the curve begins to rise, rising steeply as higher lift values are developed.

Up to separation C_{Dp} for the skeg part is assumed to be 0.02 for all skeg angles (β).

After the onset of separation aft of the skeg, C_{Dp} for the rudder plus skeg is assumed to be represented by an equation of the form

$$C_{Dp} = f(\beta) + f(\beta, C_L^5)$$

in which the first function represents the C_{Dp} value immediately after the onset of separation and the second function represents the further increase in C_{Dp} at high C_L values. A suitable relationship for the skeg plus all-movable case, which fits the data, is of the form :

$$C_{Dp} = \left[0.11 - \frac{0.1}{1 + \frac{10}{\beta + 15}}\right] + \left[\left(1 - \frac{\beta}{30}\right) \times 0.12\ C_L{}^5\right]$$

$$C_{Dp} = 0.11 - \frac{\beta + 15}{10(\beta+25)} + \left[1 - \frac{\beta}{30}\right] \times 0.12\ C_L{}^5$$

Since, for this purpose, it can be assumed that the skeg part and the all-movable part each constitutes approximately half of the total area, then removing the all-movable contribution results in the following equation for the skeg portion alone

$$C_{Dp} = 0.203 - \frac{\beta + 15}{5(\beta+25)} + \left[1 - \frac{\beta}{15}\right] \times 0.12\ C_L{}^5 \quad \ldots(36)$$

In Section 9 it is found that the rapid increase in drag values can be satisfactorily represented by equation (38) :

$$\alpha = 5 + 0.4\ (\beta+15)$$

9. ANGLE OF ATTACK FOR ONSET OF SEPARATION

The experimental results indicate that gap flow promotes separation aft of the skeg and this process takes place over an angle of attack range of two to five degrees. The precise angle at which the onset of complete separation occurs is not clear, although the discontinuities in the lift and drag curves give a broad indication.

The angles at which the discontinuity in the

lift curve occurred were derived from the experimental data. The mean values obtained are shown in Fig.14, which indicates that the onset of separation can be satisfactorily represented by :

$$\alpha_{sep} = 4 + 0.4\ (\beta+15) \qquad \ldots(37)$$

The experimental data indicate that there is a small delay in the effect of separation on the drag curve. It was, therefore, assumed that the rapid increase in drag values occurs at :

$$\alpha = 5 + 0.4\ (\beta+15) \qquad \ldots(38)$$

It should be noted that these formulae represent a prediction of a suitable location of the discontinuity in the lift and drag curves rather than a precise indication of either the start of gap flow or the onset of complete separation aft of the skeg, although they can be taken as a realistic estimate of the latter.

The angles at which the discontinuities in the normal force curves occur for the two-dimensional flapped data of Refs.12 and 13 are also shown in Fig.14. These results demonstrate a similar trend to the present work. Whilst a larger delay in the separation for the gaps sealed condition of these results might have been expected, this has been offset by the effects of the larger load produced by the 2-D section at a given angle of attack. Due to the relatively small influence of flap size indicated by this data, corrections to equations (37) and (38) for the effect of flap size were not considered necessary.

10. PROPORTION OF LOAD CARRIED BY THE MOVABLE PART AFT OF SKEG

The detailed pressure measurements which were carried out provided (locally) the ratio of flap load to total load for Rudder No.1, which had an average effective

flap ratio of 0.70; mean values of these results are shown plotted in Fig.15. The data indicate that the proportion of the load carried by the movable part, C_{Nm}/C_{Nt}, does not lend itself to a simple mathematical formulation, due mainly to dissimilar conditions for negative skeg angles. Equations were, therefore, fitted to the curves for each β value.

Refs.12 and 13 were investigated to provide further data for the influence of flap size on $C_{Nm}/_{Nt}$. The results derived from these references indicated similar trends with change in δ as those shown in Fig.15, but finding a suitable method of incorporating the influence of flap size on C_{Nm}/C_{Nt} proved difficult. The general form of the pressure distribution for the flapped foil did, however, lead to an approximate but suitable correction method. Namely, the typical pressure distribution is considered as being made up of two component parts, forward and aft of the hinge, and to have the simplified (dotted) distribution shown in Fig.16. On this assumption the ratio : flap load/total load would be $C_f/(2-C_f)$ for a total chord of unity.

Based on this reasoning the 50% and 80% chord values of C_{Nm}/C_{Nt} from Refs.12 and 13 were plotted to a base of $(C_f/(2-C_f)$; these results indicated that, at a particular angle of attack, the data could be satisfactorily represented by the relationship :

$$C_{Nm}/C_{Nt} = \text{const.} \times \frac{C_f}{(2-C_f)}$$

where the constant had a value ranging from approximately 0.8 at $\delta = 5^\circ$ and 10° up to unity at $\delta = 30^\circ$.

This property is applied as a correction to the results of Fig.15 by assuming that, at a particular angle of attack :

$$C_{Nm}/C_{Nt} \propto \left[\frac{C_f}{(2-C_f)}\right] \qquad \ldots(39)$$

The correction to the equations in Fig.15 (which are for an effective flap ratio of 0.7) therefore

becomes :

$$C_{Nm}/C_{Nt} = \left[\frac{C_{Nm}}{C_{Nt}}\right]_{0.7} \times \left[\frac{C_f}{(2-C_f)}\right] \times \left[\frac{(2-C_f)}{C_f}\right]_{0.7}$$

for $\frac{C_f}{c} = 0.7$, $\left[\frac{C_f}{(2-C_f)}\right]_{0.7} = 0.538$

hence

$$\frac{C_{Nm}}{C_{Nt}} = \left[\frac{C_{Nm}}{C_{Nt}}\right]_{0.7} \times \frac{C_f}{(1.076 - 0.538 \times C_f)} \qquad \ldots(40)$$

Whilst this correction is approximate, the investigation of the results of Refs.12 and 13 indicated that it reflects expected trends very well. It is, therefore, not expected to introduce significant errors in the relatively limited range of flap size (between, say, 60% and 75% chord) likely to occur in a parametric study of skeg size.

11. CENTRE OF PRESSURE

11.1 Spanwise CPs

This is obtained directly from a spanwise numerical integration of the load distribution.

11.2 Chordwise CPc_f for Skeg (or flapped) part

The results of the pressure measurements, Ref.3, indicated that the local CPc values are generally similar to those to be expected in two-dimensional flow (Fig.7).

Mean values of CPc_f for the movable part (flap) were obtained from the pressure measurements for Rudder No.1. This rudder has an average effective flap ratio of 0.70. These results are shown in Fig.17 and a suitable equation which represents this family of curves is :

$$CPc_f = 54 - 0.22\ (3 - 0.06\beta - 0.1\delta)^5 \qquad \ldots(41)$$

In order to provide more general data for varying flap sizes (e.g. to account for any change in flap size due to change in skeg configuration) the results of Refs.12 and 13 for 50% and 80% chord flaps were investigated. The CPc_f values with change in δ and β obtained from these references showed very similar trends to those of Fig. 17; there were some differences in absolute values although this was to be expected since the gaps were sealed for these experiments, and sharp pressure peaks were, therefore, obtained at the hinge axis.

In order to investigate the results for different flap sizes in a non-dimensional form the data from Refs.12 and 13 were re-analysed in terms of the ratio : distance of centre of pressure aft of hinge (CP_f) divided by the flap size (C_f). This analysis revealed that there were insignificant differences in CP_f/C_f between the 50% and 80% chord cases, indicating that the form of the pressure distribution over the flap at a particular angle of attack is very similar for different flap sizes. This useful result allows the basic form of equation (41) to be extended to allow for any small changes (between, say, 60% - 75% chord flap) likely to occur in a parametric study of skeg size.

Equation (41) (for an effective flap of 70% chord) can be non-dimensionalised in terms of flap size as :

$$\left[\frac{CP_f}{C_f}\right] = 0.343 - 0.00314\ (3 - 0.06\beta - 0.1\delta)^5 \qquad \ldots(42)$$

Hence, assuming CP_f/C_f to be independent of flap size, CPc_f for any flap size can be written as :

$$CPc_f = \left[\frac{CP_f}{C_f}\right] \times C_f + (100 - C_f)$$

hence :

$$CPc_f = \left[0.343 - 0.00314\ (3 - 0.06\beta - 0.1\delta)^5\right] \times C_f + (100 - C_f) \qquad \ldots(43)$$

(where CPc_f and C_f are expressed as a percentage of the total chord)

Insufficient published experimental data exists to quantify the influence of aspect ratio on CPc for aerofoils with large flaps. However, in Ref.25, the theory of Ref.26 is used to demonstrate the influence of flap size on CPc (for small angles of attack) and the theory indicates that in the aspect ratio range 2 to 4 the change in CPc position for a 70% chord flap is zero and for a 60% chord flap is 1%. These predicted small changes would account for the general similarities between the two-dimensional results of Refs.12 and 13 used earlier and those of the present work. In view of the above findings, no aspect ratio correction has been applied to equation (43).

11.3 Chordwise CPc for the All-Movable part

The pressure measurements (Ref.3) indicate values with a generally similar magnitude, and movement with α, to those expected for the aspect ratio tested, e.g. such as those available in Ref.20 and the tests on simulated all-movable rudders in Ref.1. It is seen from Fig.18 that skeg angle has very little influence on the CPc of the all-movable part.

These values, together with adjustments to allow for the small influence of change in aspect ratio (which has been derived from the data in Ref.20) are, therefore, applied to the all-movable part of the rudder. The relationship obtained from the data in Fig.18 (and its aspect ratio correction) and applied for local CPc to the inner part of the all-movable section of the rudder is :

$$CPc = 11.7 + 0.18\alpha^{1.4} + 0.7(AR-3) \qquad \ldots(44)$$

The influence of the tip vortex is to move the local chordwise centre of pressure aft, and this was illustrated in Ref.3 by the pressure distributions near the tip. The pressure distributions indicate that this effect has an influence over the outer 10% (approx) of the span, and that it displaces the CPc aft by a mean amount of approximately 8.5% for all angles. The local CPc over the

outer 10% of the span is, therefore, assumed to be of the form

$$CPc = 20.2 + 0.18\alpha^{1.4} + 0.7(AR-3) \quad \ldots(45)$$

11.4 Corrections to CPc for L.E. Sweep and Taper

In the analysis program the section CPc values derived in 11.2 and 11.3 are corrected for leading edge sweep and taper and numerically integrated across the span to yield (for the movable rudder alone) the mean $CP\bar{c}$ as a percentage of the mean chord ($\bar{c}$) aft of the L.E. of $\bar{c}$.

12. ANALYSIS COMPUTER PROGRAM

The theoretical analysis, embracing the basic lifting line theory together with the necessary adjustments and empirical corrections, was incorporated in a computer program.

For given input values of aspect ratio, taper ratio, skeg depth/span, leading edge sweep, mean flap size in way of skeg, skeg angle β and rudder angle α the program is capable of outputting the spanwise distribution of lift and normal force for the rudder plus skeg, together with its integration for total forces and spanwise CPs. The total force on the movable rudder alone is also calculated together with the chordwise $CP\bar{c}$ for the movable rudder alone.

A more detailed account of the program is given in APPENDIX 1.

13. DISCUSSION OF THE THEORETICAL RESULTS

13.1 The results of the spanwise load predictions, together with the experimental results derived from the pressure measurements, are given in Fig.19. It is seen that the correlation between theory and experiment for the overall form of the distributions is good. Agreement in magnitude was achieved by empirical correction.

The results show the skeg incidence reduction approach to satisfactorily predict the measured changes in load distribution due to change in skeg angle.

The changes in load near the tip, with change in incidence, show that it is reasonable to assume the tip vortex effect to be a function of α^2.

Because the pressure distributions were deficient (by up to 5% at 20° and 30°) the form of the lift predictions by theory were compared with the normal forces from pressure measurements. The differences between the total normal and lift forces amount to about 3% at $\alpha = 10^\circ$ and 20° and up to 5% at $\alpha = 30^\circ$ and hence have a small effect on the form of the distributions shown in Fig.19. Using this approach the integration of the theoretical distributions will, of course, lead to total forces closer to those obtained by direct force measurement.

13.2 Figs.20(a) to (e) show the results of the integrations of the spanwise distributions for load and centre of pressure, superimposed on the direct force measurements. As would be expected, following the good agreement with the spanwise distributions, the lift predictions are also satisfactory.

It is worthy of note that, whilst the values of γ were derived by correlating with the pressure measurements for $\beta = 0, \pm 5^\circ$ (together with other theoretical and experimental data), the extrapolation of these predictions to $\beta = \pm 10^\circ$ (Figs.20(a) and (e)) is also very satisfactory.

The profile drag was estimated from the experimental results. The satisfactory predictions of total drag indicate, therefore, that the induced drag predicted by the analysis is of the correct order of magnitude.

The CP predictions are generally reasonable, although CPs is deficient for most skeg angles and CP$\bar{c}$ is forward of the results from the dynamometer measurements up to about $\alpha = 15^{\circ}$.

The CPs values show the correct trends with changes in incidence and the deficiencies are generally the same as those for the integrated pressure results; as mentioned in the discussion of the direct force and pressure measurements (Refs.3 and 5) some error could in any case exist in the CPs values from the dynamometer measurements at the lower angles of incidence. The deficiencies in CPs do, however, suggest that too much emphasis was placed on correlating the theoretical spanwise distributions with those from the pressure measurements; for example, better agreement with the CPs values from the force measurements could have been achieved by using slightly larger γ values and an increased lift curve slope correction factor.

The empirical CP$\bar{c}$ values also show the correct general order of travel with change in incidence; the forward position at low incidence was obtained with the pressure measurements and is likely to be also due to the fairing of the data of Fig.17. Because the required trends were reflected reasonably well, no further attempts at modifying the empirical CP$\bar{c}$ results were pursued.

13.3 Figs.21(a) and (b) show the predicted influence of taper ratio compared with the experimental results, for one skeg angle. Reasonable correlation for C_L and C_D was achieved by the empirical corrections applied, although the values of C_L for T = 0.8 were slightly over-estimated whilst those for T = 1.0 were slightly under-estimated.

The errors in the $CP_{\bar{c}}$ predictions for small incidence are generally similar to those for T = 0.6 (Figs.20(a) to (e)) discussed earlier.

The large error in the CPs predictions for Rudder No.2 with T = 0.8 (Fig.21(a)) is due to the high values derived from the dynamometer measurements. This irregularity (of CPs for Rudder No.2 being greater than that for Rudder No.3) is discussed in Ref.5.

13.4 It should be noted that the analysis considers rudder angles up to 30°, and no attempt is made to predict stall.

The analysis was developed for, and is hence limited to, ranges of skeg angle up to $\pm 10^{\circ}$, aspect ratio 2 to 4, taper ratio 0.5 to 1.0, skeg depth 0.36S to 0.63S and mean movable flap 60% to 75% chord.

Within the limits considered in the present analysis, the results shown in Figs.19, 20 and 21 demonstrate that, whilst the theoretical approach used is simple and heavily modified empirically, it gives very realistic predictions of skeg rudder performance characteristics.

13.5 The scope of the present work did not allow a full exploration of the possible flexibility of the analysis method. For example, as a check, removal of the mid-span vortex and setting $\gamma = 0$ in the analysis program leads to all-movable C_L predictions close to the experimental values.

Also, setting the γ value in the program to that for no separation aft of the skeg (equation 26) for all angles of incidence leads to C_L predictions close to the experimental values for sealed vertical gaps.

14. PARAMETRIC STUDY

14.1 INTRODUCTION

A parametric study was carried out to provide a limited extension to the experimental data. Predictions of the changes in performance with changes in the principal rudder and skeg characteristics were made using the computer program which incorporated the modified theoretical span loading analysis and empirical formulae.

14.2 SCOPE OF STUDY

The number of possible variations in rudder characteristics is, in theory, infinite. However, in practical terms, skeg chord and hence skeg area is to a certain extent dependent on structural requirements, and balance area is dependent on both skeg area and sweep. The chosen variations in the principal characteristics were, therefore, restricted to realistic limits of these features (the extent of the theoretical and empirical analysis was in any case limited to practical boundaries). Similarly, the study was restricted to representative rudder and skeg angles of $\alpha = 10^{\circ}$ and 20° for $\beta = 0^{\circ}, \pm 5^{\circ}$.

The chosen parametric variations shown in Figs.23 to 26 attempt to give a broad outline of the expected changes in performance with changes in skeg and rudder particulars, and to highlight the problems faced when choosing suitable skeg proportions.

The particular notation for the skeg, used in the presentation, is given in Fig.22. Due to practical

requirements of thickness and gap, the centreline of the stock is about 6% aft of the L.E. of the mean effective flap chord. This criterion was, therefore, used in the development of the theory and in the theoretical analysis program.

14.3 DISCUSSION OF RESULTS

14.3.1 Figs.23 and 24 show the influence of skeg depth and movable chord for taper ratios of 0.6 and 0.8 respectively.

It is seen that, for constant C_f, increase in skeg depth has a detrimental effect on lift coefficient, particularly at the larger angle of attack; for example, increasing the skeg depth ratio from 0.45 to 0.55 leads to a 3% loss in lift at 10° and an 8% loss in lift at 20°. Differences between the results would be expected on account of the dependence of γ on α as well as δ for the 20° (separated) condition, whereas $\alpha = 10^\circ$ represents the case before separation aft of the skeg. It is also seen that skeg depth has an influence on $CP\bar{c}$ (for constant C_f), an increase in skeg depth from 0.45 to 0.55 leading to about $3\%\bar{c}$ aft movement of $CP\bar{c}$ for both $\alpha = 10^\circ$ and 20°.

14.3.2 Figs.23 and 24 show that change in the movable chord size (C_f) has a significant effect on C_L and $CP\bar{c}$ at $\alpha = 10^\circ$ where, for $S_1/S = 0.5$, an increase in C_f/c from 0.65 to 0.75 (Fig.23(a)) leads to a 4% increase in lift and a 2% aft movement of $CP\bar{c}$; at $\alpha = 20^\circ$ the influence of C_f on $CP\bar{c}$ is similar to that at 10° but the influence on C_L is very small. The influence on C_L is reversed for $\alpha = 10^\circ$ and 20° and this is due to the contrary effects on γ before and after separation.

For both angles of attack the movable chord size has a marked influence on the stock position, skeg area and hence balance; for example, in Fig.24(b), a change in C_f/c from 0.6 to 0.7 leads to a forward movement of stock of about 10% compared with a forward movement in $CP\bar{c}$ of only about 2%.

14.3.3 In Fig. 25 one value of skeg depth ($S_1/S = 0.5$) is considered and the influences of C_f/c and sweep are investigated for $\alpha = 20^\circ$. The influence of C_f/c on C_L and $CP\bar{c}$ is relatively small for the larger angle of attack (as was concluded from Figs. 23(b) and 24(b)) whereas it has a marked influence on the stock position and balance area.

If it is assumed that $CP\bar{c}$ is to coincide with the stock position at $\alpha = 20^\circ$ then for a sweep of 0.153 rads the required balance ratio is approximately 20.5% and $C_f/c = 0.65$ whereas for 0.070 rads sweep the required C_f/c rises to 0.695 and the balance ratio is again about 20.5%.

Similarly, from Fig.24(b), if C_L is increased by decreasing skeg depth, and a large disparity between $CP\bar{c}$ and the stock position is to be avoided, the balance ratio has to be held at approximately 20.5% and C_f/c has to be increased from about 0.6 at $S_1/S = 0.63$ to about 0.7 at $S_1/S = 0.36$.

It is thus clearly seen that if an increase in performance is to be achieved by decreasing skeg depth then this has to be accompanied by a decrease in skeg chord (or an increase in L.E. sweep if structural requirements limit the decrease in skeg chord).

Figs 23 and 24 indicate that skeg depth has a very small effect on CPs.

The influence of skeg depth on C_D is negligible at $\alpha = 10^\circ$ although at 20° there was a marked decrease in C_D with increase in skeg depth; this trend is in the same sense as C_L and, for clarity, C_D has been omitted from the plottings.

14.3.4 The C_L values for $\beta = \pm 5^o$ are superimposed on Figs.24(a) and (b) and it is seen that the trends are similar to $\beta = 0^o$, with the influence of skeg depth being slightly larger for negative skeg angle.

14.3.5 Fig.26 shows that the influence of aspect ratio on C_L at a particular skeg depth is generally similar to that expected for all-movable control surfaces. The influence of skeg depth on C_L is seen to be independent of aspect ratio. For $T \neq 1$ and $\Omega_1 \neq 0$, Fig.26 indicates that as aspect ratio is decreased for constant values of taper ratio, skeg depth ratio, flap chord ratio and sweep, the skeg area ratio remains fixed, $CP\bar{c}$ moves forward by a small amount and the stock position moves aft by a significant amount; thus, for constant sweep, an increase in flap chord ratio (hence decrease in skeg area ratio) is required with decrease in aspect ratio if the torque lever is to remain approximately constant.

14.3.6 Figs.23(a) and 24(a) or 23(b) and 24(b) indicate that the influence of skeg depth for different taper ratios is generally similar.

14.3.7 It may be concluded that, for fixed aspect ratio and taper ratio, the production of sideforce is significantly influenced by the size of the skeg depth and movable chord (hence skeg chord) at lower angles of attack and by the skeg depth at larger angles of attack.

Variation in skeg depth has a marked effect on balance area and $CP\bar{c}$ at small and large rudder angles.

For a particular skeg depth the movable chord and sweep have a relatively small influence on $CP\bar{c}$ whereas they have a large influence on the stock position and balance area, hence having a marked effect on the magnitude of torque over the incidence range; careful choice of these dimensions, in association with a particular skeg depth, is, therefore, necessary.

15. CONCLUSIONS

(i) The earlier experimental investigation demonstrated that a skeg rudder exhibits a number of particular characteristics which affect the prediction or assessment of its performance. The experimental results, supported by the present theoretical analysis, showed that changes in the skeg angle, for a particular rudder angle, lead to changes in local lift in way of the skeg and at the same time have a significant effect on the all-movable portion of the rudder. Realistic predictions of load are, therefore, not likely to be achieved by assuming the skeg rudder to be made up of separate flapped and all-movable parts.

(ii) The experimental spanwise load distributions revealed a high loading near the tip and undulations in the distribution near the break between the skeg and all-movable parts. It was concluded that both these features were due to particular trailing vortices being generated at these positions. The influence of the tip vortex is particularly significant and non-linear, and it is clear that this effect cannot be neglected if realistic span loads are to be predicted for small aspect ratio rudders with square tips.

(iii) The theoretical study demonstrated that satisfactory predictions of the form of the spanwise loadings for different skeg and rudder angles can be made using lifting line theory, with the effect of the skeg being incorporated as local incidence reduction and the effects of the mid-span and tip trailing vortices being incorporated as twist corrections to the local incidence. The correct magnitude of the distributions was satisfactorily reproduced by applying, spanwise, a single empirical correction based on the ratio of the experimental and theoretical lift curve slopes.

(iv) The theoretical and empirical extensions to the experimental work demonstrated that a decrease in the skeg depth leads to an increase in lift production; it follows that the best hydrodynamic performance will be achieved by minimising this dimension to the limits of structural requirements.

Decrease in skeg chord leads to an improvement in lift at low angles of attack; however, choice of this dimension (and sweep) for a particular skeg depth will depend primarily on achieving a suitable stock position and balance area.

The influence of aspect ratio on skeg rudder performance was found to be similar to that expected from an all-movable rudder, and to be independent of skeg depth.

Increase in taper ratio leads to small improvements in lift at larger angles of attack due primarily to the effect of removing area from the less efficient part of the rudder aft of the skeg to the more efficient 'all-movable' part of the rudder. This improvement is accompanied by a small movement of the centre of pressure towards the tip, with consequent increase in bending moment.

NOTATION

A	Total rudder area (movable rudder plus skeg)
A_E	Effective area (2 x A)
AR	Effective aspect ratio
AR_G	Geometric aspect ratio
a	Lift curve slope correction factor
A_n, a_n, b_n	Coefficients in Fourier series for spanwise load distribution
B_A	Balance area ratio
c	Chord
C_T	Tip chord
C_R	Root chord
$\bar{c}$	Mean chord $((C_T + C_R)/2)$
C_f	Flap chord
CPc	Local (or section) centre of pressure chordwise, %c, measured from L.E.
$CP\bar{c}$	Total centre of pressure chordwise, %$\bar{c}$, measured from L.E.
CP_f	Centre of pressure of flap aft of hinge
CPc_f	Centre of pressure of flap aft of L.E. of chord
CPs	Centre of pressure spanwise, %S, measured from root
C_D	Drag coefficient $(D/\frac{1}{2}\rho AV^2)$
C_{Di}	Induced drag coefficient
C_{Dp}	Profile drag coefficient
C_L	Lift coefficient $(L/\frac{1}{2}\rho AV^2)$
C_N	Total normal force coefficient, normal to rudder $(N/\frac{1}{2}\rho AV^2) = C_L Cos\alpha + C_D Sin\alpha)$
C_{Nm}	Local normal force coefficient on the movable part of the rudder in way of skeg (based on total chord)
C_{Nt}	Local total normal force coefficient in way of skeg
D	Drag force in direction of air flow
$H_1(\theta)$	General form of downwash variation induced by tip vortex
$H_2(\theta)$	General form of downwash variation induced by mid-span vortex
k	Defined as (1-T) in lifting line analysis

L	Lift force normal to air flow
m	Two-dimensional lift curve slope
N	Normal force, normal to centreline of movable rudder
n	Number of control points in lifting line analysis
S	Rudder span
S_1	Skeg depth
S_A	Skeg area ratio
T	Taper ratio (C_T/C_R)
V	Inflow velocity
x	Distance to centreline of stock from L.E. of rudder ($\%\bar{c}$)
y	Spanwise co-ordinate in lifting line analysis
α	Rudder angle relative to flow (Fig.3)
α_i	Downwash angle
α_T	Equivalent local twist
$\bar{\alpha}$	Defined as $(\alpha-\gamma)$ in lifting line analysis
α_{sep}	Approx. angle at which onset of separation occurs aft of skeg
β	Skeg angle relative to flow, or ship drift angle at rudder (Fig.3)
γ	Skeg incidence reduction in lifting line analysis
Γ	Circulation
δ	Rudder angle relative to skeg, or ship (Fig.3)
θ	Spanwise co-ordinate in lifting line analysis
μ	Coefficient in lifting line analysis
ν	Kinematic viscosity
ρ	Mass density
φ	Value of θ at end of skeg
Ω	Sweep of quarter chord
Ω_1	Sweep of leading edge
ω	Induced normal velocity

$$\text{Skeg Area Ratio } (S_A) = \frac{\text{Skeg area (assumed to } \text{¢} \text{ of stock)}}{\text{Total Area (movable + skeg)}}$$

$$\text{Balance Area Ratio}(B_A) = \frac{\text{Movable area forward of } \text{¢} \text{ of stock}}{\text{Total Movable Area}}$$

$$\text{Total Movable Area} = \text{Total area (movable + skeg) - skeg area (assumed to } \text{¢} \text{ of stock)}$$

REFERENCES

1. Molland A.F. : 'The Free-Stream Characteristics of a Semi-Balanced Ship Skeg-Rudder'. University of Southampton, Ship Science Report No.3/77, 1977.

2. Molland A.F. : 'Further Free-Stream Characteristics of Semi-Balanced Ship Skeg-Rudders'. University of Southampton, Ship Science Report No.2/78, 1978.

3. Molland A.F. : 'Pressure-Distribution Investigation of a Semi-Balanced Ship Skeg Rudder'. University of Southampton, Ship Science Report No.5/81, 1980.

4. Goodrich G.J. and Molland A.F. : 'Wind Tunnel Investigation of Semi-Balanced Ship Skeg-Rudders'. Trans. R.I.N.A., Vol.121, 1979.

5. Molland A.F. : 'The Free-Stream Characteristics of Ship Skeg-Rudders'. Ph.D. Thesis, Faculty of Engineering and Applied Science, University of Southampton, 1982.

6. Robinson A. and Laurmann, J.A. : 'Wing Theory'. Cambridge University Press.

7. Glauert H. : 'The Elements of Aerofoil and Airscrew Theory'. Cambridge University Press.

8. Hopkins E.J. : 'Lift, Pitching Moment and Span Load Characteristics of Wings at Low Speeds as affected by Variations of Sweep and Aspect Ratio'. N.A.C.A., T.N.2284, 1951.

9. Glauert H. : 'Theoretical Relationships for an Aerofoil with Hinged Flap'. A.R.C., R & M No.1095, 1927.

10. Hoerner S.F. and Borst H.V. : 'Fluid - Dynamic Lift'. Publ. by Mrs. L.A. Hoerner, 1975.

11. Ames M.B. Jr. and Sears R.I. : 'Pressure - Distribution Investigation of an N.A.C.A. 0009 Airfoil with a 30-Percent-Chord Plain Flap and Three Tabs'. T.N. No.759 N.A.C.A. 1940.

12. Street W.G. and Ames M.B. Jr. : 'Pressure - Distribution Investigation of an N.A.C.A. 0009 Airfoil with a 50-Percent-Chord Plain Flap and Three Tabs'. T.N. No.734 N.A.C.A. 1939.

13. Ames M.B. Jr. and Sears R.I. : 'Pressure - Distribution Investigation of an N.A.C.A. 0009 Airfoil with an 80-Percent-Chord Plain Flap and Three Tabs'. T.N. No.761 N.A.C.A. 1940.

14. Sears R.I. : 'Wind Tunnel Investigation of Control Surface Characteristics. I - Effect of Gap on the Aerodynamic Characteristics of an N.A.C.A. 0009 Airfoil with a 30-Percent-Chord Plain Flap'. Report L-377, N.A.C.A., June 1941.

15. Küchemann D. : 'Types of Flow on Swept Wings, with Special Reference to Free Boundaries and Vortex Sheets'. J.R. Aero Soc., Vol.57, November 1953.

16. Cheng H.K. : 'Aerodynamics of a Rectangular Plate with Vortex Separation in Supersonic Flow'. J. Aero. Sc., Vol.22, April 1955.

17. Küchemann D. : 'A Simple Method for Calculating the Span and Chordwise Loading on Straight and Swept Wings of any Given Aspect Ratio at Subsonic Speeds'. A.R.C., R & M No.2935, 1952.

18. Weber J., Küchemann D. and Brebner G.G. : 'Low Speed Tests on 45° Swept Back Wings, Parts I and II'. A.R.C., R & M 2882, 1951.

19. Küchemann D. and Kettle D.J. : 'The Effect of Endplates on Swept Wings'. A.R.C., C.P.No.104, 1952.

20. Whicker L.F. and Fehlner L.F. : 'Free Stream Characteristics of a Family of Low Aspect Ratio Control Surfaces for Application to Ship Design'. D.T.M.B. Report 933, December 1958.

21. Flax A.H. and Lawrence H.R. : 'The Aerodynamics of Low-Aspect-Ratio Wings and Wing-Body Combinations'. Third Int. Conf., Brighton, 1951.

22. Betz A. : 'Applied Airfoil Theory'; Aerodynamic Theory, Vol.IV. W.F. Durand, Editor, J. Springer, 1935.

23. Abbot I.H. and Von Doenhoff A.E. : 'Theory of Wing Sections'. Dover Publications, New York, 1958.

24. Jones G.W. Jr. : 'Aerodynamic Characteristics of Three Low Aspect Ratio Symmetrical Wings with Rectangular Planforms at Reynolds Numbers between 0.4×10^6 and 3.0×10^6. N.A.C.A. R.M. L52G18, 1952.

25. Campbell I.J., Blanks C.F. and Lever D.A. : 'Aerodynamic Characteristics of Rectangular Wings of Small Aspect Ratio'. A.R.C., R & M No.3142, 1956.

26. Lawrence H.R. : 'The Lift Distribution on Low Aspect Ratio Wings at Subsonic Speeds'. J. Aero. Sc., Vol.18, October 1951.

APPENDIX 1.

DESCRIPTION OF THE THEORETICAL ANALYSIS COMPUTER PROGRAM

An analysis program was written which incorporated the modified theoretical span loadings and empirical formulae. The program was written in Basic and run on a Tektronix 4052 machine.

A prediction assuming no separation aft of the skeg at larger angles can be made by modifying the program whereby the 'unseparated' value of γ (eqtn.26) is applied throughout the incidence range.

An all-movable rudder prediction can be made by setting the skeg incidence reduction γ and the mid vortex distribution $H_2(\theta)$ to zero in the program.

A brief outline of the program steps and a listing of the program are given on the following pages.

Outline of Steps in Analysis Program

Required input information

- AR, T, skeg depth, mean flap chord, L.E. sweep, α and β (Allowable skeg depth/span ratios: .36, .43, .50, .57, .63 (Fig.37); allowable β values: 0, ± 5, ± 10 for any α).
- $H_1(\theta)$ and $H_2(\theta)$ distributions retained in program as data statements.
- Derive spanwise control stations $\theta = I\pi/2N$, for N = 20, I = 1 to 20.
- Derive number of control stations in way of skeg for application of γ.
- Recover α_T, using eqtns.(28) and (29).
- Calc. flap chord ratio across skeg.
- Calc. γ using eqtns.(26) or (27).
- Calc. distribution of $(\bar{\alpha} + \alpha_T)$.
- Solve Fourier coeff'ts of eqtn.(7). (20 coeff'ts from 20 values of θ).
- Correct Fourier coeff'ts by factor, a.
- Derive spanwise stations and multipliers; rudder treated non-dimensionally in two parts (skeg section and all-movable section) in order to facilitate numerical integration and allow variation in skeg depth.
- Calc. span. distri. of lift using corrected Fourier coeff'ts and eqtn.(9).
- Calc. span. distri. of net downwash, eqtn.(16).
- Calc. span. distri. of C_{Di} eqtn.(17).
- Calc. span. distri. of C_{Do} using eqtns.(35) and (36).
- Calc. span. distri. of C_D.
- Calc. prop'n of load carried by movable flap, eqtn.(40).
- Calc. span. distri. of CPc, eqtns.(43), (44), (45).
- Numerical integration for total coeff'ts and centres of pressure; i.e. C_L, C_N, C_D, CPs for rudder + skeg, and C_{NR}, CP$\bar{c}$ for movable rudder alone.

```
100 REM MODIFIED LIFTING LINE ANALYSIS FOR SKEG RUDDERS
120 DIM P(20),A0(20),A2(20),G0(20),R(20),A(20)
140 DIM X(20,21),Y(20,21)
160 DIM R1(20),R2(20),B(20),H1(20),H2(20)
180 DIM H(6),Z0(25),S0(25),L1(25),P1(25),C3(25),C4(25)
200 DIM A3(25),G1(20),Z5(20),Z6(20),E4(25),R5(25),G2(20)
220 DIM D2(25),D3(25),D4(25),N5(25),W0(25)
240 DIM X1(25),X2(25)
260 READ N,M
280 READ S,T,G5,S1,E0
300 C=2/(1+T)
320 IF S1=0.36 THEN 420
340 IF S1=0.43 THEN 460
360 IF S1=0.5 THEN 500
380 IF S1=0.57 THEN 540
400 IF S1=0.63 THEN 580
420 N1=15
440 GO TO 600
460 N1=14
480 GO TO 600
500 N1=13
520 GO TO 600
540 N1=12
560 GO TO 600
580 N1=11
600 K=1-T
620 E=M*C/(8*S)
640 FOR I=1 TO N
660 P(I)=I*3.142/(2*N)
680 Z5(I)=COS(P(I))
700 NEXT I
720 L=1
740 FOR J=1 TO N
760 FOR I=1 TO N
780 X(I,J)=SIN(L*P(I))*(E*L+SIN(P(I))/(1-K*COS(P(I))))
800 NEXT I
820 L=L+2
840 NEXT J
860 FOR I=1 TO 20
880 X(I,21)=0
900 NEXT I
920 Y=INV(X)
940 READ A1
960 READ B1
980 D1=A1-B1
1000 E3=(2-S1+S1*T)*(1-E0)/(1+T)
1020 FOR I=N1+1 TO N
1040 Z6(I)=(E3+S*G5*(S1/2-Z5(I)))*(1+T)/(2-Z5(I)+2*Z5(I)*T)
1060 Z6(I)=1-Z6(I)
1080 IF A1>4+0.4*(B1+15) THEN 1180
1100 E1=0.48/100*(Z6(I)*100*(100-Z6(I)*100))^0.5
1120 E2=ASN((Z6(I)*100)^0.5/10)
1140 G1(I)=D1*(1-2/3.142*(E1+E2))
1160 GO TO 1200
1180 G1(I)=0.3*A1-3+0.39*D1+0.4*(Z6(I)-0.7)*(28-D1)
1200 NEXT I
1220 FOR I=1 TO N
1240 READ H1(I)
1260 A0(I)=A1+H1(I)*(A1*A1/10)*(3*1/(2*S))*T^1.5/0.465
1280 NEXT I
1300 FOR I=1 TO 17-N1
1320 READ H(I)
1340 NEXT I
1360 FOR I=1 TO N1
1380 READ H2(I)
1400 IF D1<0 THEN 1460
1420 G0(I)=0+H2(I)*D1^0.5*A1^0.5*2
1440 GO TO 1480
1460 G0(I)=0-H2(I)*(-1*D1)^0.5*A1^0.5*2
1480 NEXT I
1500 FOR I=N1+1 TO N
1520 READ H2(I)
1540 IF D1<0 THEN 1600
1560 G0(I)=G1(I)+H2(I)*D1^0.5*A1^0.5*2
1580 GO TO 1620
1600 G0(I)=G1(I)-H2(I)*(-1*D1)^0.5*A1^0.5*2
1620 NEXT I
1640 FOR I=1 TO N1-9
1660 READ H(I)
1680 NEXT I
1700 FOR I=1 TO N
1720 R1(I)=E*A0(I)*SIN(P(I))/57.3
1740 R2(I)=E*G0(I)*SIN(P(I))/57.3
1760 NEXT I
1780 PRINT @4:
1800 PRINT @4:
1820 PRINT @4:
1840 E5=E0-0.06
1860 E6=(2-S1+S1*T)*(1-E5)/(1+T)
1880 E7=E6*S1
1900 E7=INT(1000*E7+0.5)/10
1920 E8=(2*E6-S*G5)*(1-S1)/((1-E6*S1)*2)
1940 E8=INT(1000*E8+0.5)/10
1960 E9=E6+S*G5*(S1-1)/2
1980 E9=INT(1000*E9+0.5)/10
2000 PRINT @4:"EFFECTIVE ASPECT RATIO=";2*S,"TAPER RATIO=";T
2020 PRINT @4:"SKEG DEPTH/SPAN=";S1,"MEAN FLAP CHORD RATIO=";E0
2040 PRINT @4:"L.E. SWEEP(RADS)=";G5,"STOCK POSITION AFT L.E.=";E9
2060 PRINT @4:"SKEG AREA RATIO=";E7,"BALANCE AREA RATIO=";E8
2080 PRINT @4:
2100 PRINT @4:"SKEG ANGLE(BETA)=";B1
```

```
2120 PRINT @4:"RUDDER ANGLE(ALPHA)=";A1
2140 A9=T^0.1/0.95*0.875*(1.14*2*S+2)/(2*S+3.9)
2160 PRINT
2180 GO TO 2220
2200 PRINT "FOURIER COEFFICIENTS"
2220 FOR F=1 TO N
2240 A(F)=0
2260 B(F)=0
2280 I=1
2300 FOR J=1 TO N
2320 A(F)=A(F)+Y(F,J)*R1(I)
2340 B(F)=B(F)+Y(F,J)*R2(I)
2360 I=I+1
2380 NEXT J
2400 A(F)=A(F)*A9
2420 B(F)=B(F)*A9
2440 GO TO 2480
2460 PRINT A(F),B(F)
2480 NEXT F
2500 REM START OF DERIVATION OF STATIONS AND MULTIPLIERS----------
2520 P0=1
2540 I1=0
2560 FOR I=1 TO 11
2580 Z0(I)=0+I1*S1/10
2600 S0(I)=3-P0
2620 P0=-P0
2640 I1=I1+1
2660 NEXT I
2680 S0(1)=S0(1)/2
2700 S0(11)=S0(11)/2
2720 P0=1
2740 I1=11
2760 FOR I=12 TO 20
2780 Z0(I)=Z0(11)+(1-S1)/10*(I1-11)
2800 S0(I)=3-P0
2820 P0=-P0
2840 I1=I1+1
2860 NEXT I
2880 S0(12)=S0(12)/2
2900 S0(20)=S0(20)/2
2920 P0=0.5
2940 I1=20
2960 FOR I=21 TO 25
2980 Z0(I)=Z0(20)+(1-S1)/20*(I1-20)
3000 S0(I)=1.5-P0
3020 P0=-P0
3040 I1=I1+1
3060 NEXT I
3080 Z0(25)=0.999
3100 S0(21)=S0(21)/2
3120 S0(25)=S0(25)/2
3140 REM START OF SPANWISE DISTRIBUTIONS-----------------------
3160 GO TO 3200
3180 PRINT @4:"X/S","LL","LN","D"
3200 P1(1)=1.5708
3220 FOR I=2 TO 25
3240 P1(I)=ATN((1-Z0(I)*Z0(I))^0.5/Z0(I))
3260 NEXT I
3280 FOR I=1 TO 25
3300 C3(I)=0
3320 C4(I)=0
3340 L=1
3360 FOR F=1 TO N
3380 C3(I)=C3(I)+A(F)*SIN(L*P1(I))
3400 C4(I)=C4(I)+B(F)*SIN(L*P1(I))
3420 L=L+2
3440 NEXT F
3460 L1(I)=(C3(I)-C4(I))*8*S
3480 L1(I)=INT(1000*L1(I)+0.5)/1000
3500 NEXT I
3520 FOR I=1 TO 11
3540 IF A1>5+0.4*(B1+15) THEN 3600
3560 D2(I)=0.02
3580 GO TO 3620
3600 D2(I)=0.203-(B1+15)/(5*(B1+25))+(1-B1/15)*0.12*L1(I)^5
3620 E4(I)=(E3+S*G5*(S1/2-Z0(I)))*(1+T)/(2-Z0(I)+2*Z0(I)*T)
3640 E4(I)=1-E4(I)
3660 IF A1>4+0.4*(B1+15) THEN 3760
3680 E1=0.48/100*(E4(I)*100*(100-E4(I)*100))^0.5
3700 E2=ASN((E4(I)*100)^0.5/10)
3720 G2(I)=D1*(1-2/3.142*(E1+E2))
3740 GO TO 3780
3760 G2(I)=0.3*A1-3+0.39*D1+0.4*(E4(I)-0.7)*(28-D1)
3780 A3(I)=A1-G2(I)
3800 NEXT I
3820 FOR I=12 TO 25
3840 A3(I)=A1
3860 D2(I)=0.017+0.12*L1(I)^5
3880 NEXT I
3900 FOR I=1 TO 11
3920 X1(I)=(0.343-0.00314*(3-0.06*B1-0.1*D1)^5)*E4(I)*100+100-E4(I)*100
3940 NEXT I
3960 FOR I=12 TO 20
3980 X1(I)=11.7+0.18*A1^1.4+0.7*(2*S-3)
4000 NEXT I
4020 FOR I=21 TO 25
4040 X1(I)=20.2+0.18*A1^1.4+0.7*(2*S-3)
4060 NEXT I
4080 FOR I=1 TO 25
4100 W0(I)=A3(I)/57.3-L1(I)/(M*C*(1-K*COS(P1(I))))
```

```
4120 D3(I)=L1(I)*W0(I)
4140 D4(I)=D2(I)+D3(I)
4160 N5(I)=L1(I)*COS(A1/57.3)+D4(I)*SIN(A1/57.3)
4180 N5(I)=INT(1000*N5(I)+0.5)/1000
4200 X2(I)=X1(I)*(2/(1+T))*(1-(1-T)*Z0(I))+100*G5*Z0(I)*S-100*G5*S/2
4220 GO TO 4260
4240 PRINT @4:Z0(I),L1(I),N5(I),INT(1000*D4(I)+0.5)/1000
4260 NEXT I
4280 REM START OF DERIVATION OF TOTAL COEFFICIENTS------------------
4300 IF D1>35 THEN 4340
4320 GO TO 4360
4340 D1=35
4360 IF B1=-10 THEN 4460
4380 IF B1=-5 THEN 4500
4400 IF B1=0 THEN 4540
4420 IF B1=5 THEN 4580
4440 IF B1=10 THEN 4620
4460 R0=0.62+0.12*(3.5-D1/10)^2.2
4480 GO TO 4640
4500 R0=0.7+0.022*(3.5-D1/10)^2.47
4520 GO TO 4640
4540 R0=0.68-0.023*(3.5-D1/10)^1.72
4560 GO TO 4640
4580 R0=0.59-0.013*(3.5-D1/10)^2.6
4600 GO TO 4640
4620 R0=0.54-0.015*(3.5-D1/10)^2.6
4640 FOR I=1 TO 11
4660 R5(I)=R0*E4(I)/(1.076-0.538*E4(I))
4680 NEXT I
4700 L2=0
4720 D5=0
4740 D8=0
4760 N6=0
4780 N3=0
4800 M2=0
4820 M4=0
4840 FOR I=1 TO 11
4860 L2=L2+L1(I)*S0(I)
4880 D5=D5+D3(I)*S0(I)
4900 D8=D8+D4(I)*S0(I)
4920 N6=N6+N5(I)*S0(I)
4940 N3=N3+R5(I)*N5(I)*S0(I)
4960 M2=M2+N5(I)*S0(I)*Z0(I)
4980 M4=M4+R5(I)*N5(I)*S0(I)*X2(I)
5000 NEXT I
5020 L2=L2*S1/(10*3)
5040 D5=D5*S1/(10*3)
5060 D8=D8*S1/(10*3)
5080 N6=N6*S1/(10*3)
5100 N3=N3*S1/(10*3)
5120 M2=M2*S1/(10*3)
5140 M4=M4*S1/(10*3)
5160 L3=0
5180 D6=0
5200 D9=0
5220 N7=0
5240 M3=0
5260 M5=0
5280 FOR I=12 TO 25
5300 L3=L3+L1(I)*S0(I)
5320 D6=D6+D3(I)*S0(I)
5340 D9=D9+D4(I)*S0(I)
5360 N7=N7+N5(I)*S0(I)
5380 M3=M3+N5(I)*S0(I)*Z0(I)
5400 M5=M5+N5(I)*S0(I)*X2(I)
5420 NEXT I
5440 L3=L3*(1-S1)/(10*3)
5460 D6=D6*(1-S1)/(10*3)
5480 D9=D9*(1-S1)/(10*3)
5500 N7=N7*(1-S1)/(10*3)
5520 M3=M3*(1-S1)/(10*3)
5540 M5=M5*(1-S1)/(10*3)
5560 L4=L2+L3
5580 L4=INT(1000*L4+0.5)/1000
5600 D7=D5+D6
5620 D0=D8+D9
5640 D7=INT(1000*D7+0.5)/1000
5660 D0=INT(1000*D0+0.5)/1000
5680 N8=N6+N7
5700 N8=INT(1000*N8+0.5)/1000
5720 N4=N3+N7
5740 N4=INT(1000*N4+0.5)/1000
5760 P5=(M2+M3)/N8
5780 P5=INT(1000*P5+0.5)/10
5800 P6=(M4+M5)/N4
5820 P6=INT(10*P6+0.5)/10
5840 PRINT @4:"CL=";L4,"CNT=";N8,"CNR=";N4
5860 PRINT @4:"CDI=";D7,"CD=";D0,"CPC=";P6,"CPS=";P5
5880 DATA 20,5.5
5900 DATA 1.5,0.6,0.153,0.5,0.7
5920 DATA 20
5940 DATA 0
5960 DATA 1.75,1.7,1.5,0.95,0.1,-0.13,-0.12,-0.08,-0.06,-0.04
5980 DATA -0.02,-0.01,0,0,0,0,0,0,0,0
6000 DATA 0,0,0,0,0,0,0,0,0,0,0,0,0,0.01,0.03,0.05,0.13
6020 DATA 0,-0.15,-0.02,0,0,0,0,0,0,0,0
6040 GO TO 9999
6060 WINDOW 0,0.999,0,1.2
6080 MOVE @5:Z0(1),L1(1)
6100 FOR I=1 TO 25
6120 DRAW @5:Z0(I),L1(I)
6140 NEXT I
9999 END
```

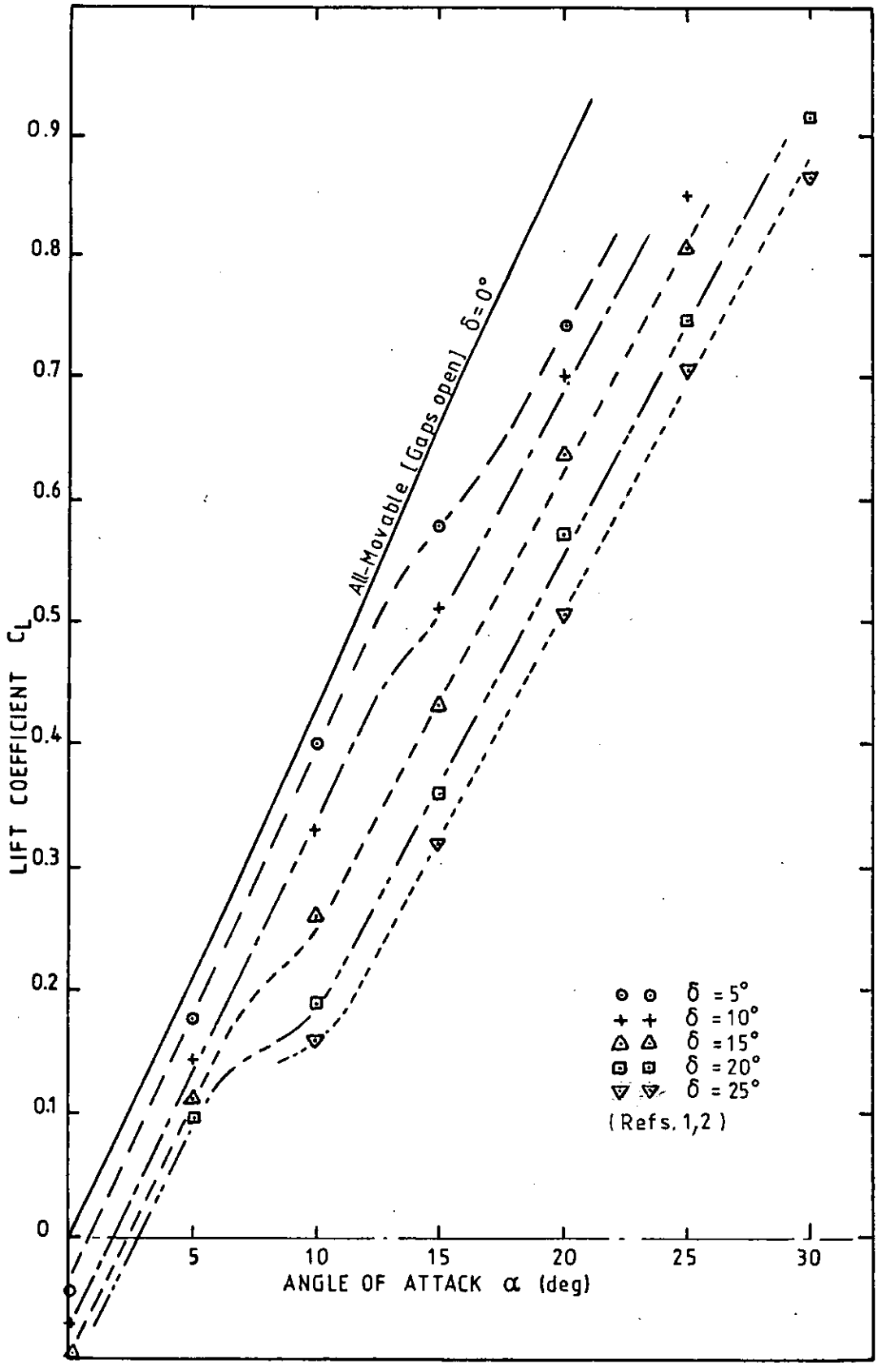

Fig. 1 LIFT CHARACTERISTICS FOR SKEG RUDDER No.1 FOR CONSTANT VALUES OF δ

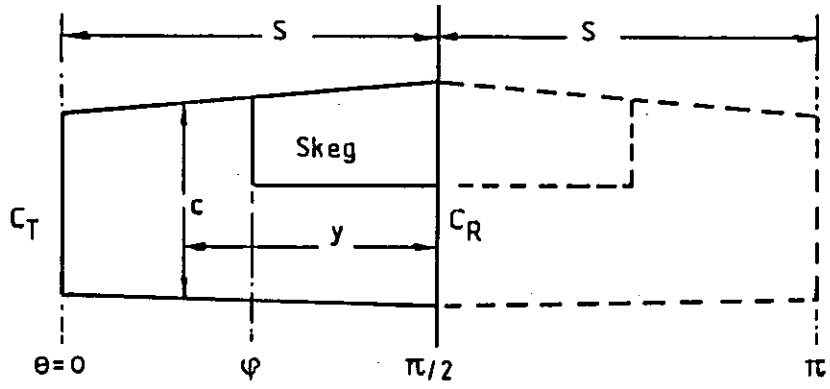

Fig. 2 RUDDER GEOMETRY USED IN ANALYSIS

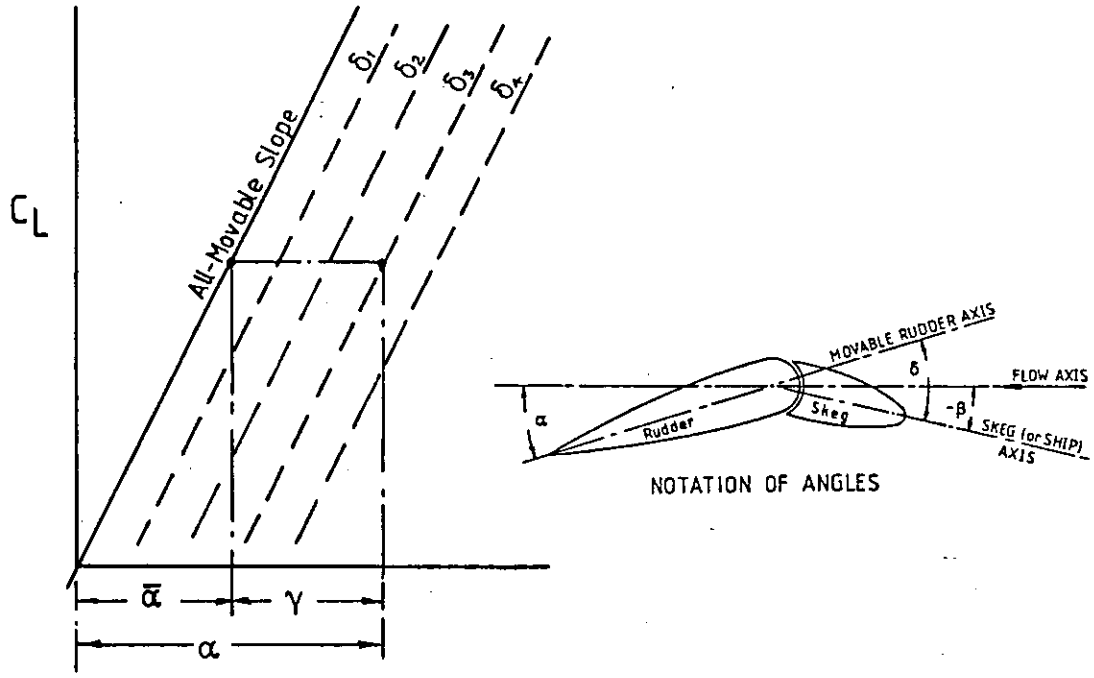

Fig. 3 APPLICATION OF γ

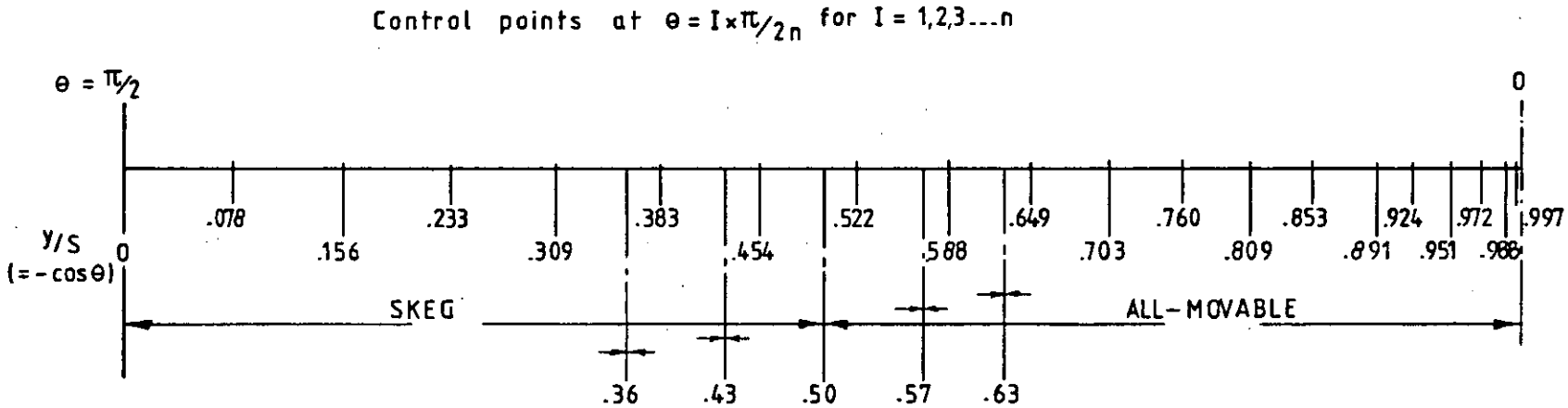

Fig. 4 POSITION OF ANALYSIS CONTROL POINTS

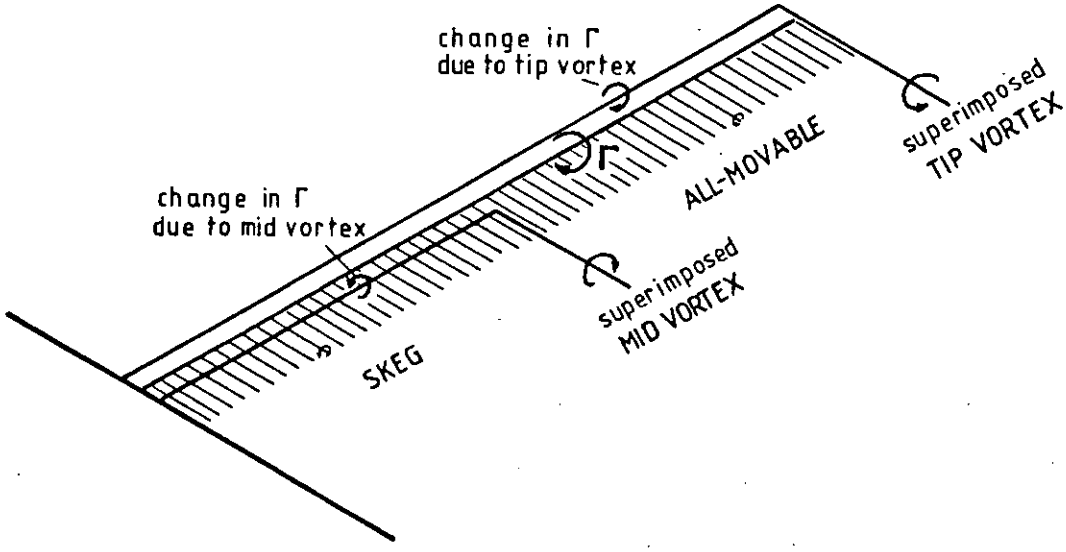

Fig. 5 BASIC VORTEX MODEL

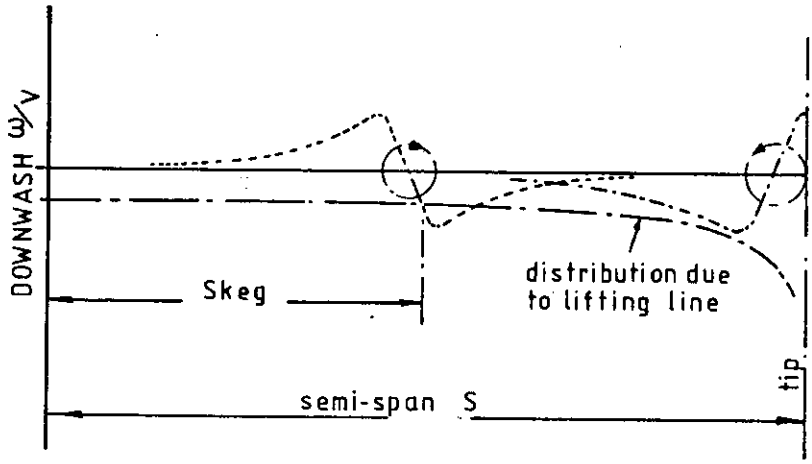

Fig. 6 DOWNWASH DISTRIBUTIONS OF ASSUMED VORTEX MODEL

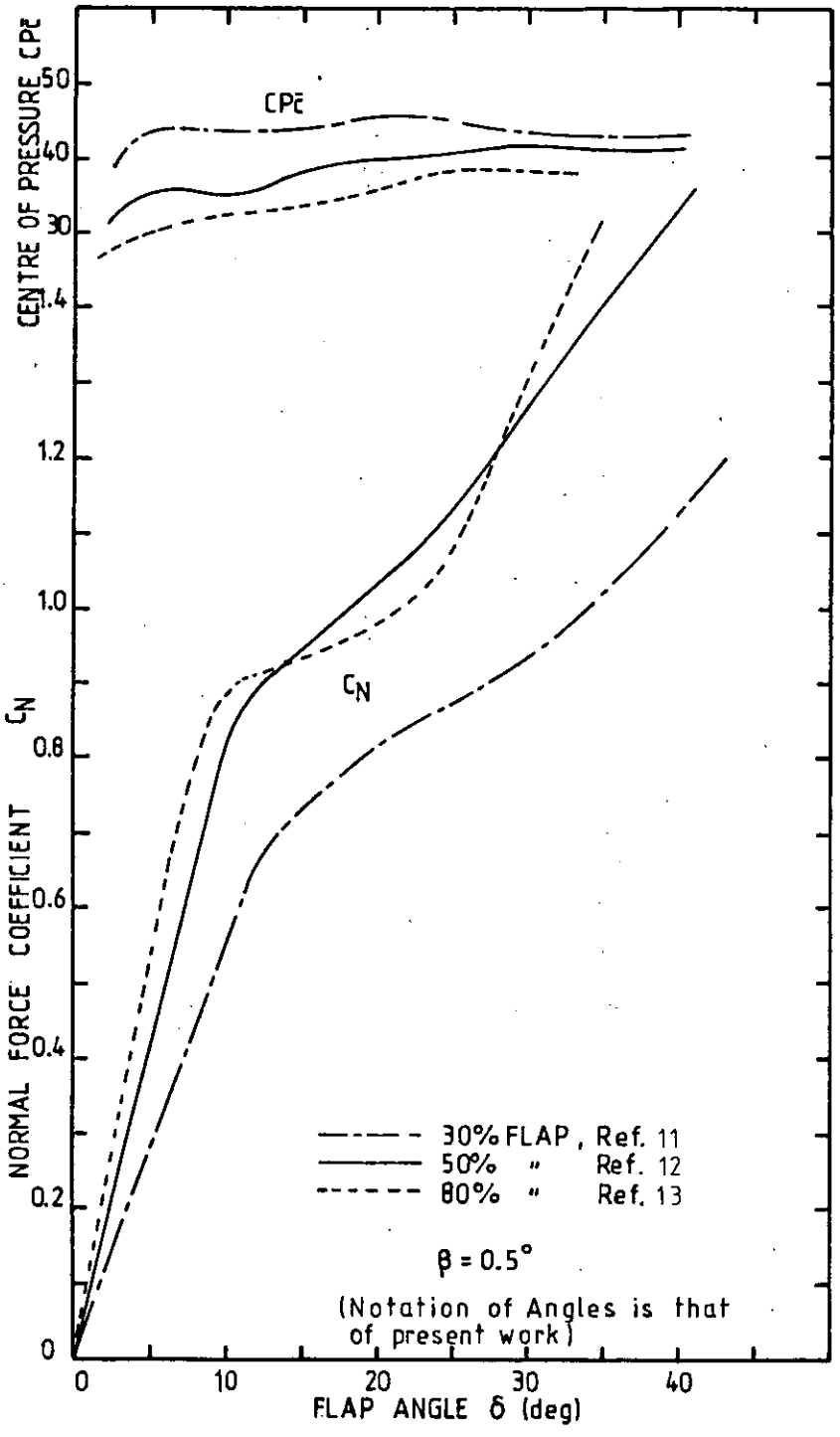

Fig. 7 TWO-DIMENSIONAL SECTION DATA FOR FLAPPED AEROFOILS (from Refs. 11,12,13)

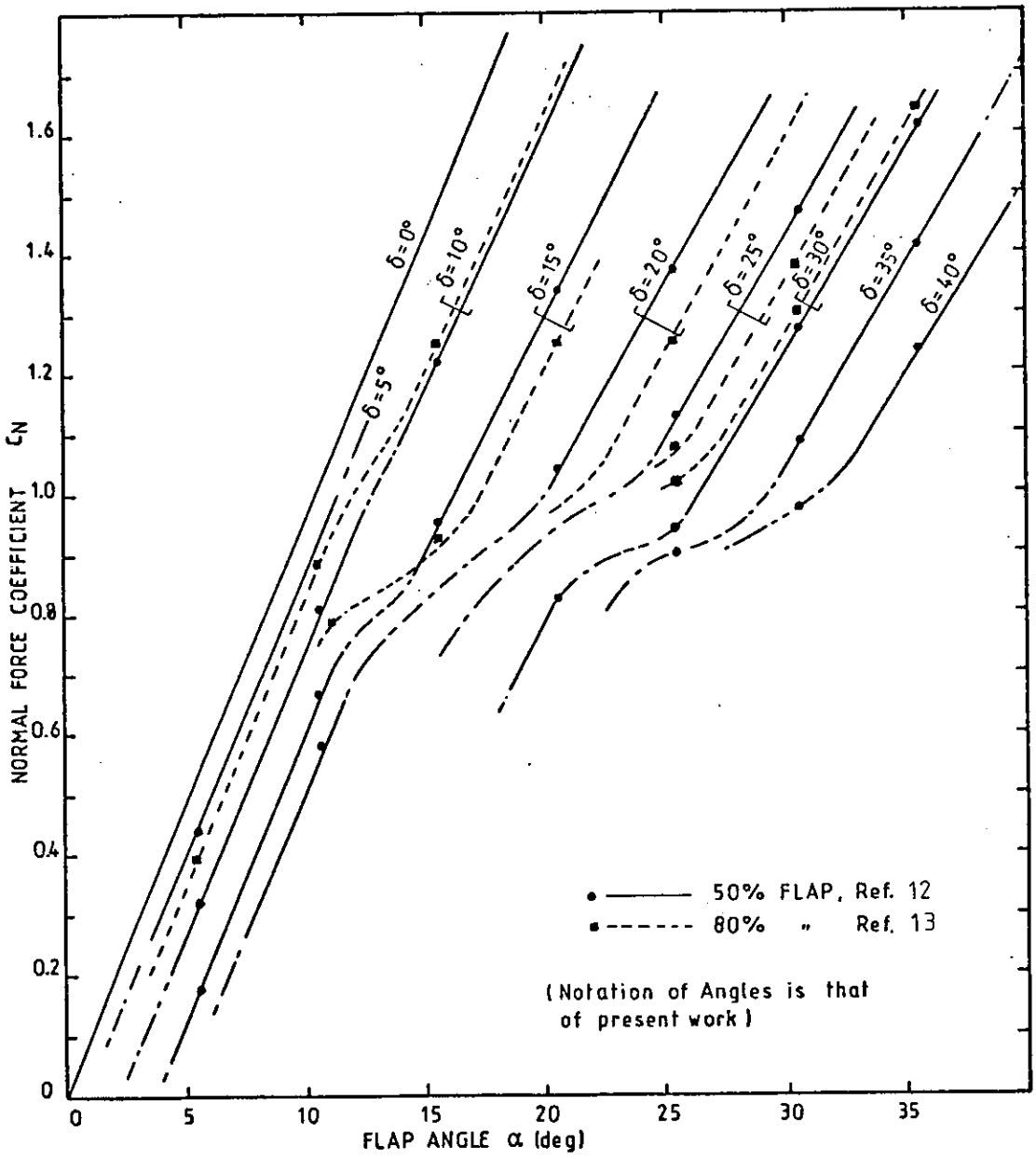

Fig. 8 TWO-DIMENSIONAL SECTION DATA FOR FLAPPED AEROFOILS (from Refs. 12,13)

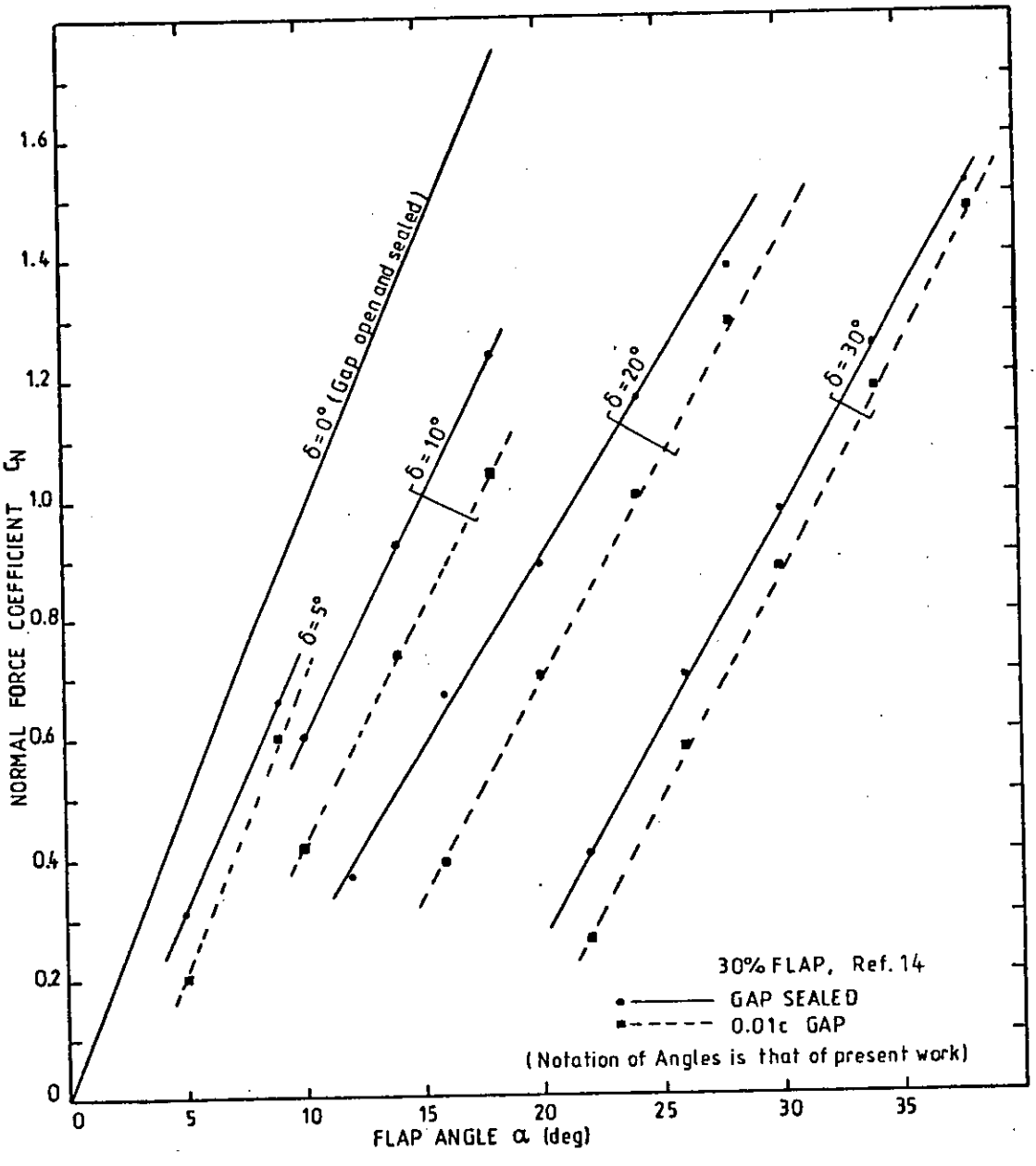

Fig. 9 TWO-DIMENSIONAL SECTION DATA FOR A FLAPPED AEROFOIL (from Ref. 14)

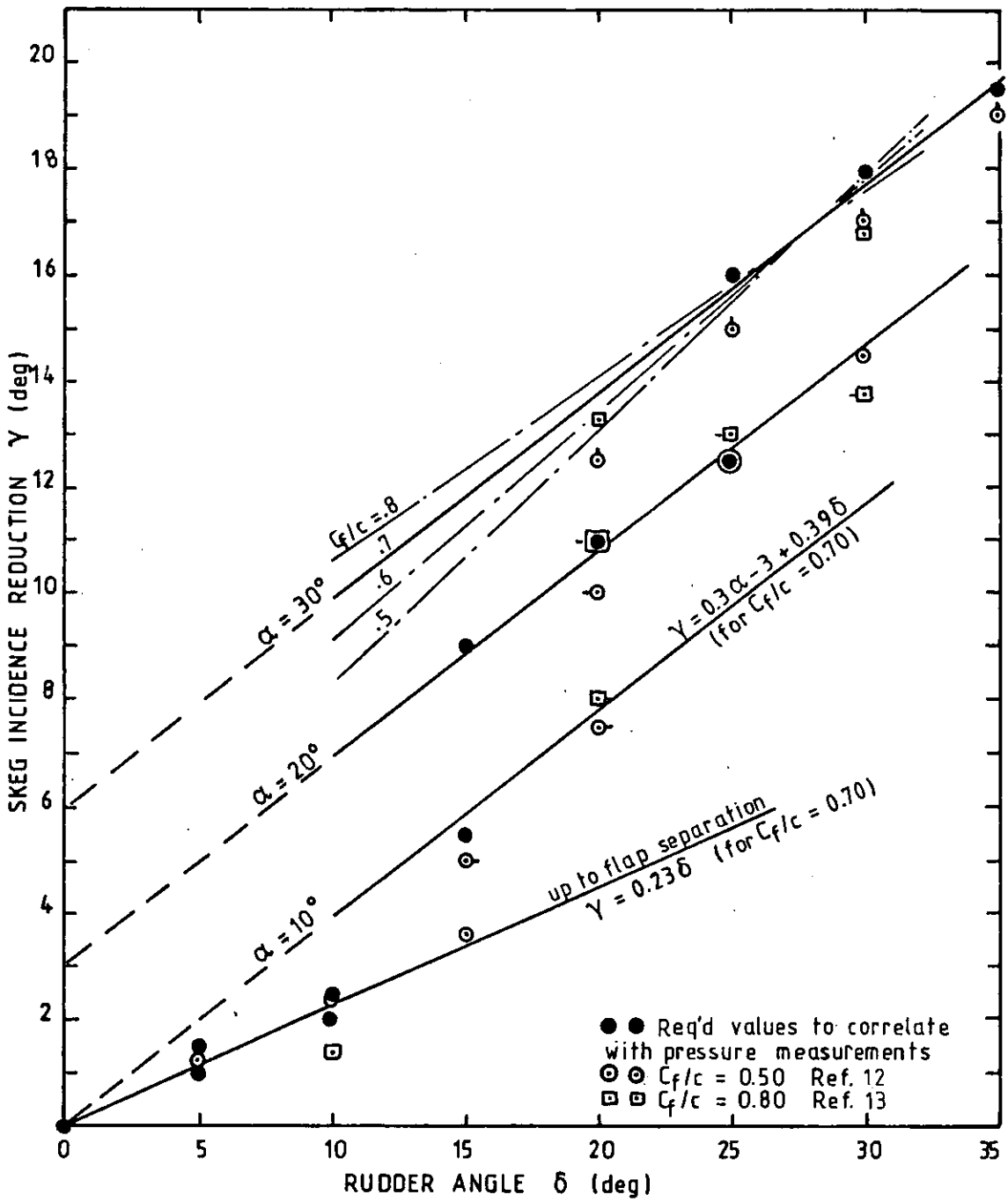

Fig. 10 SKEG INCIDENCE REDUCTION γ

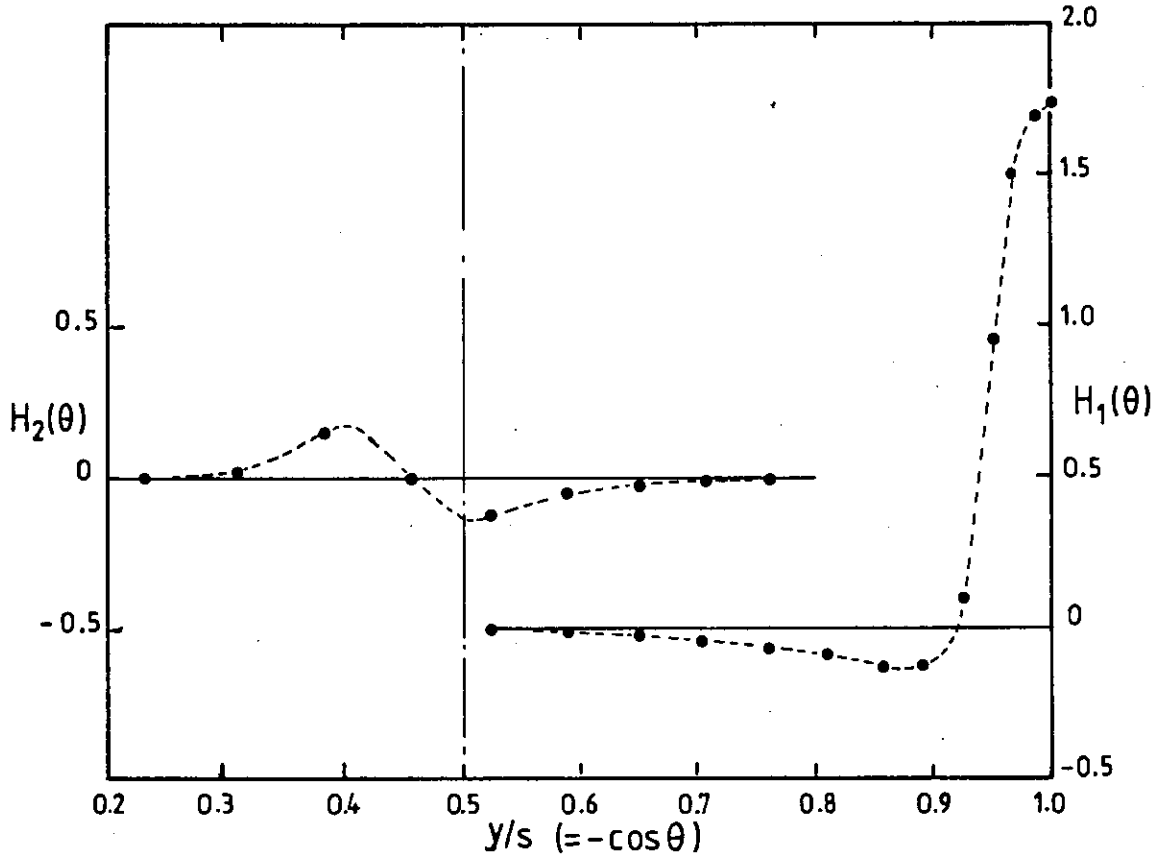

Fig. 11 GENERAL FORM OF FUNCTIONS $H_1(\theta)$ and $H_2(\theta)$

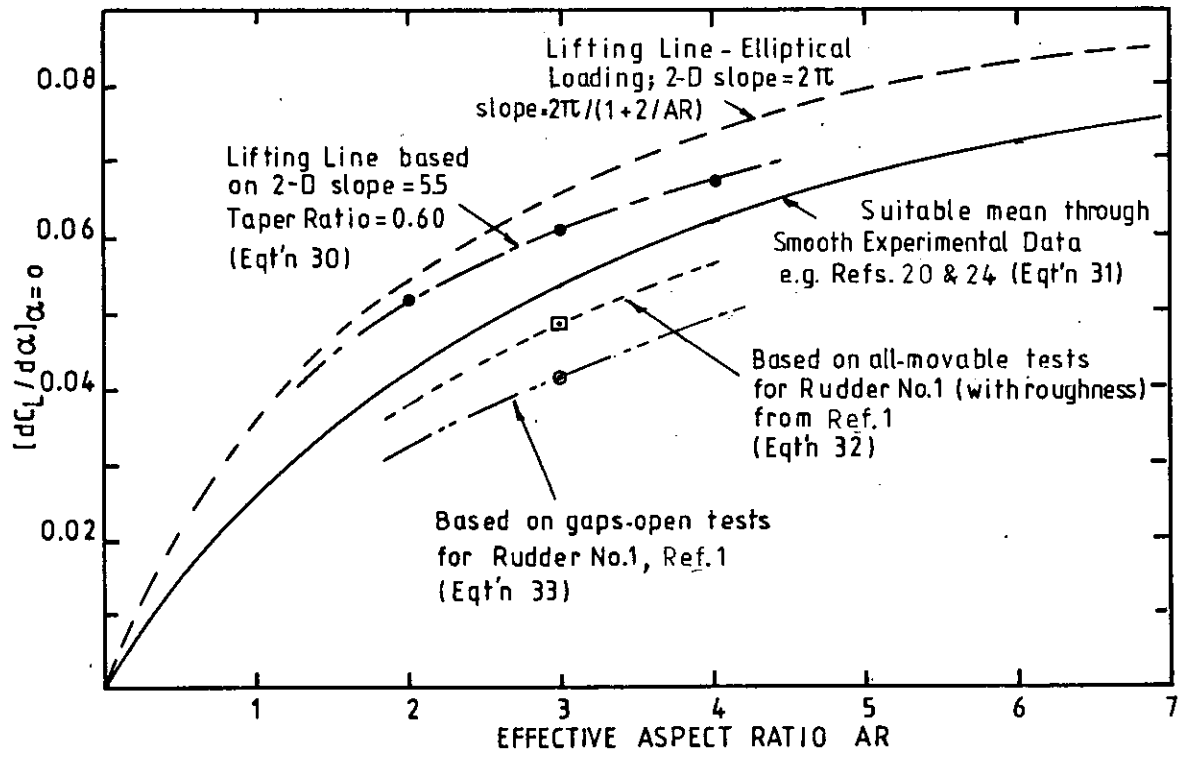

Fig. 12 LIFT CURVE SLOPES ALL-MOVABLE RUDDERS

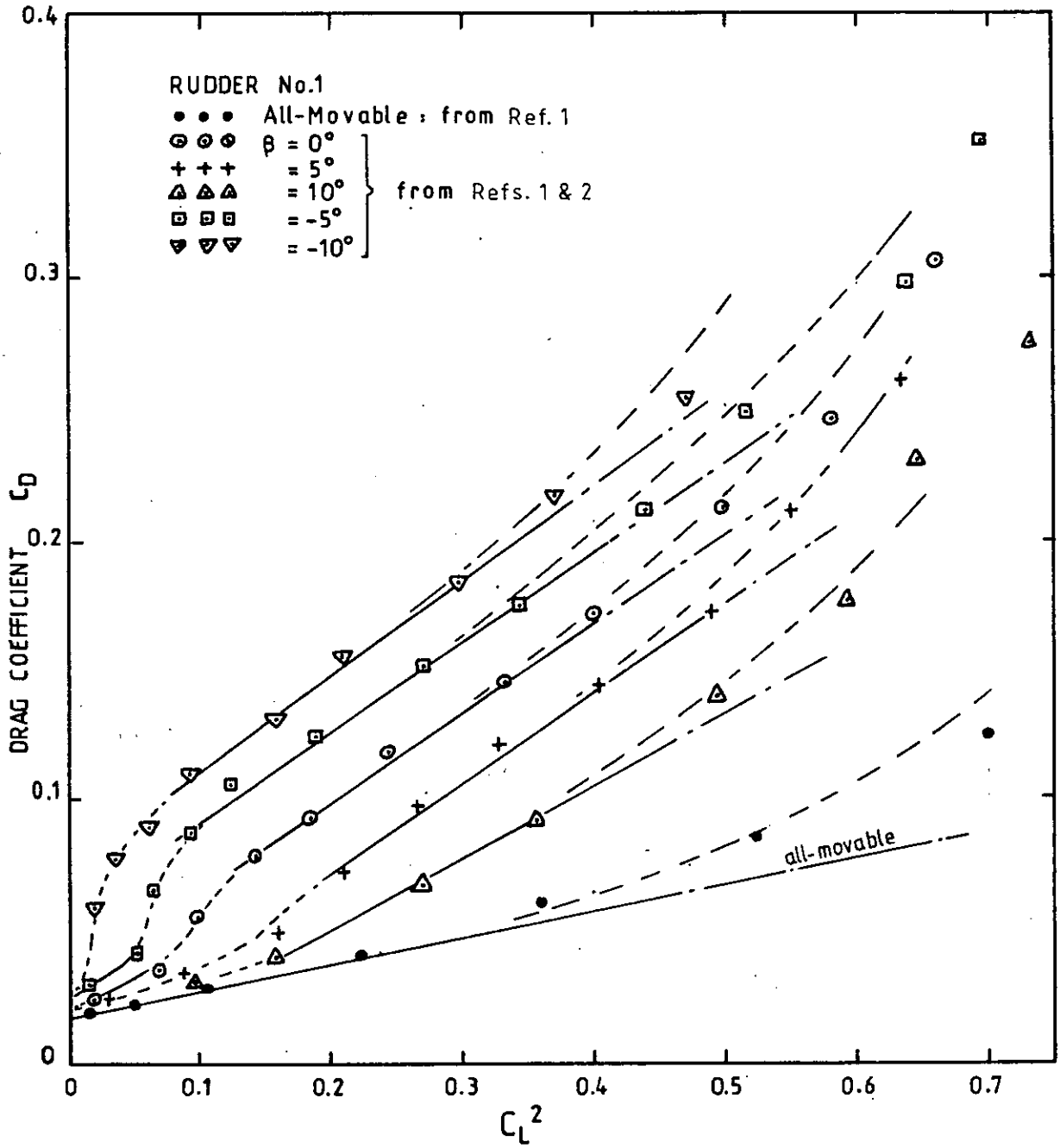

Fig. 13 DERIVATION OF PROFILE DRAG COEFFICIENT C_{Dp}

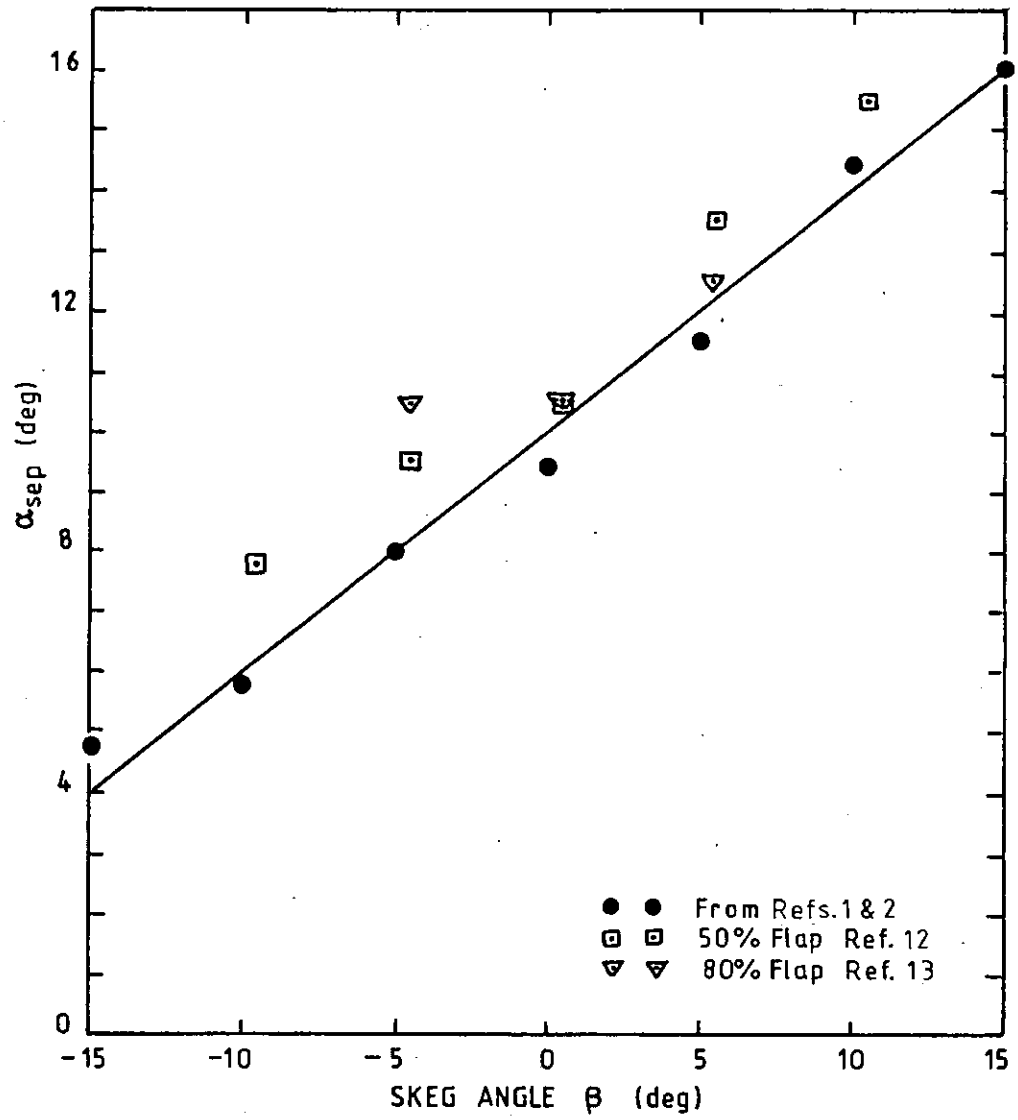

Fig. 14 α FOR ONSET OF SEPARATION AFT OF SKEG

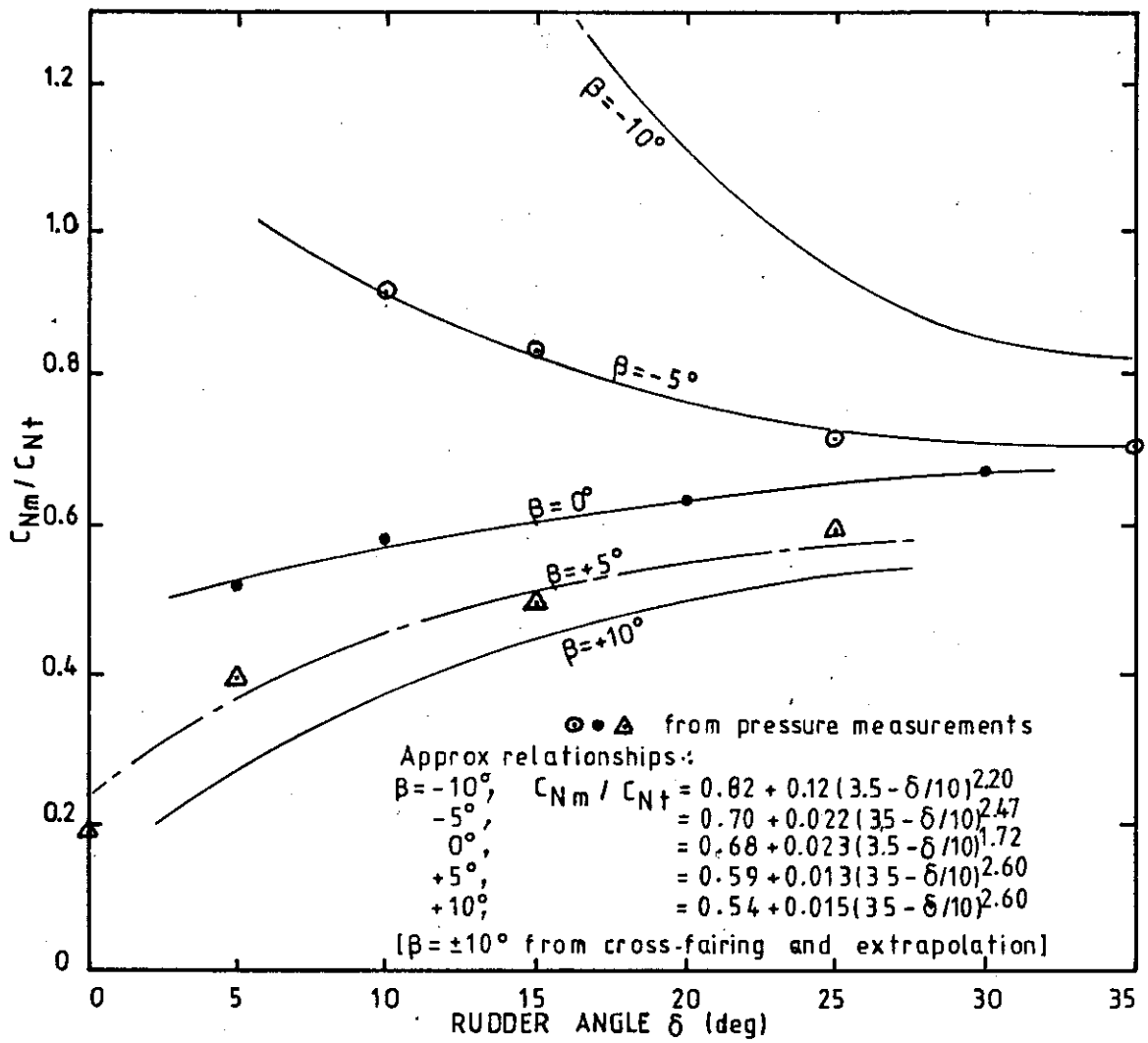

Fig. 15 RATIO OF FLAP LOAD / TOTAL LOAD

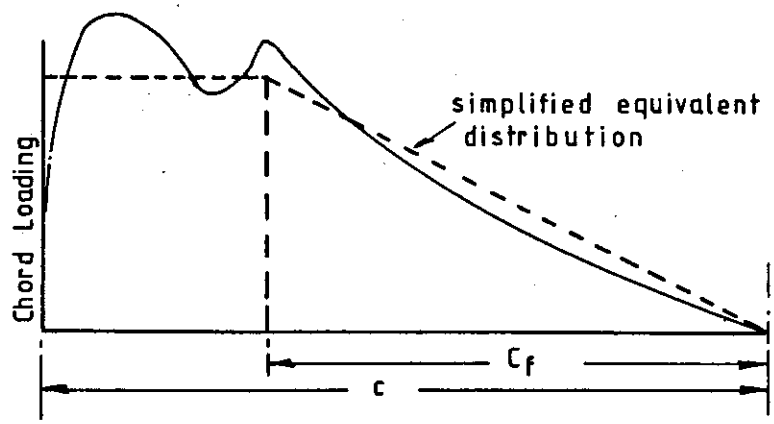

Fig. 16 EQUIVALENT CHORD LOAD DISTRIBUTION

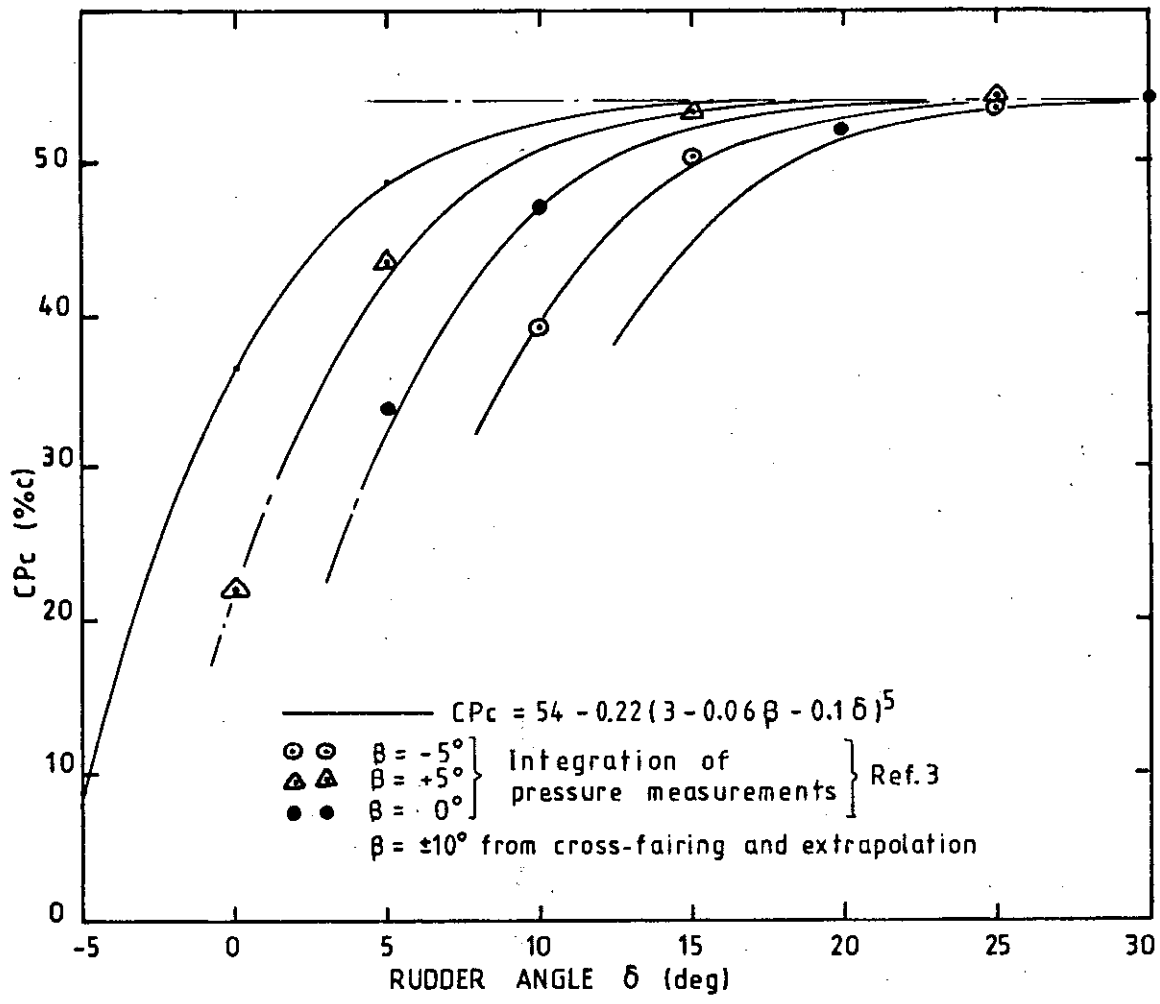

Fig. 17 CHORDWISE CENTRE OF PRESSURE: movable part aft of skeg

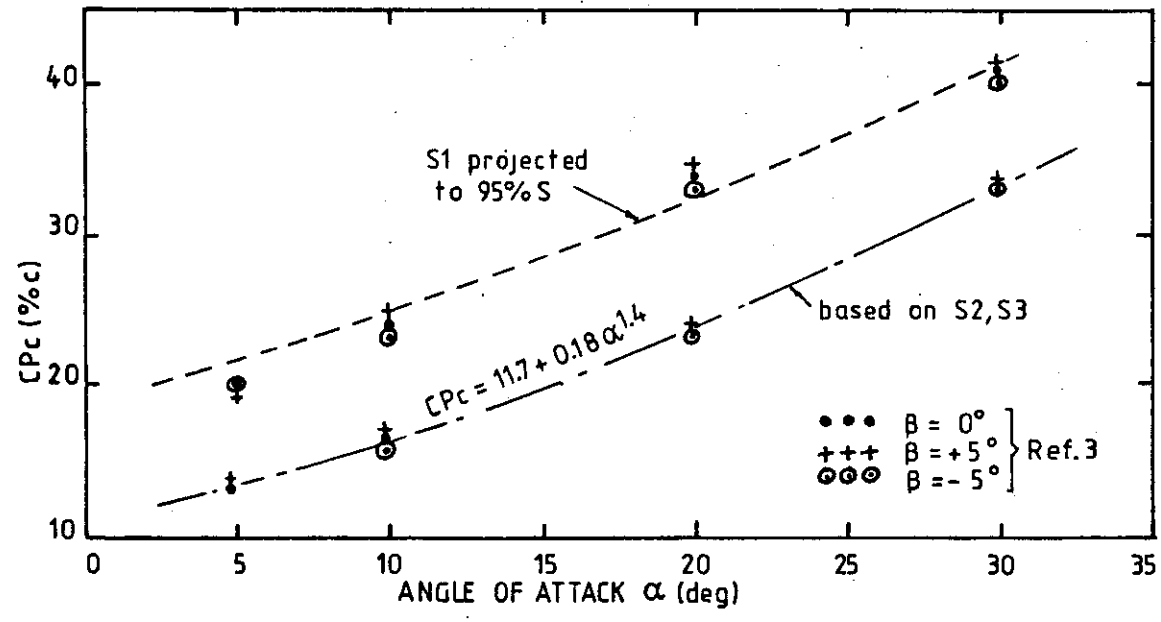

Fig. 18 CHORDWISE CENTRE OF PRESSURE: all movable part

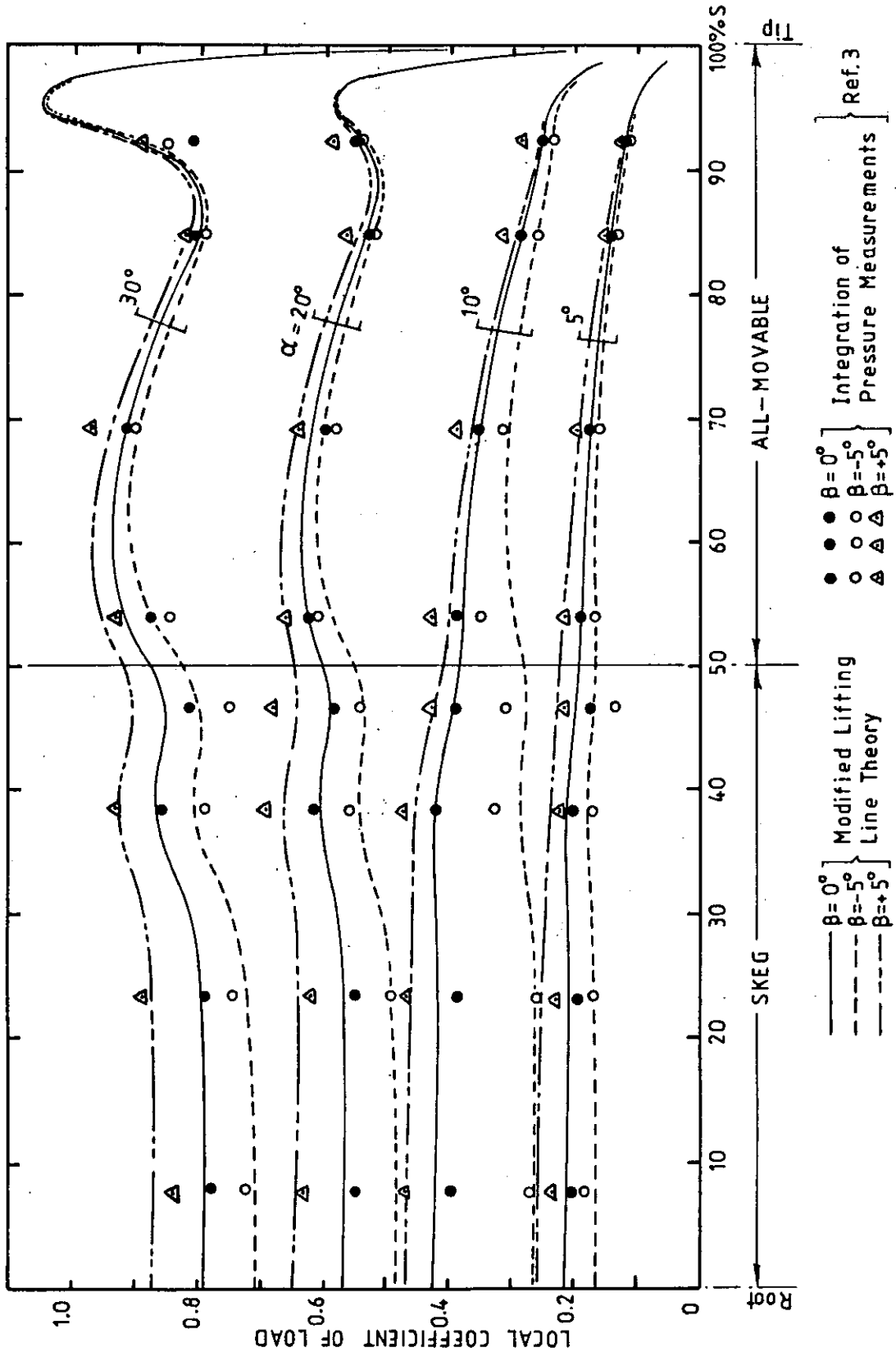

Fig. 19 THEORETICAL SPANWISE LOADINGS

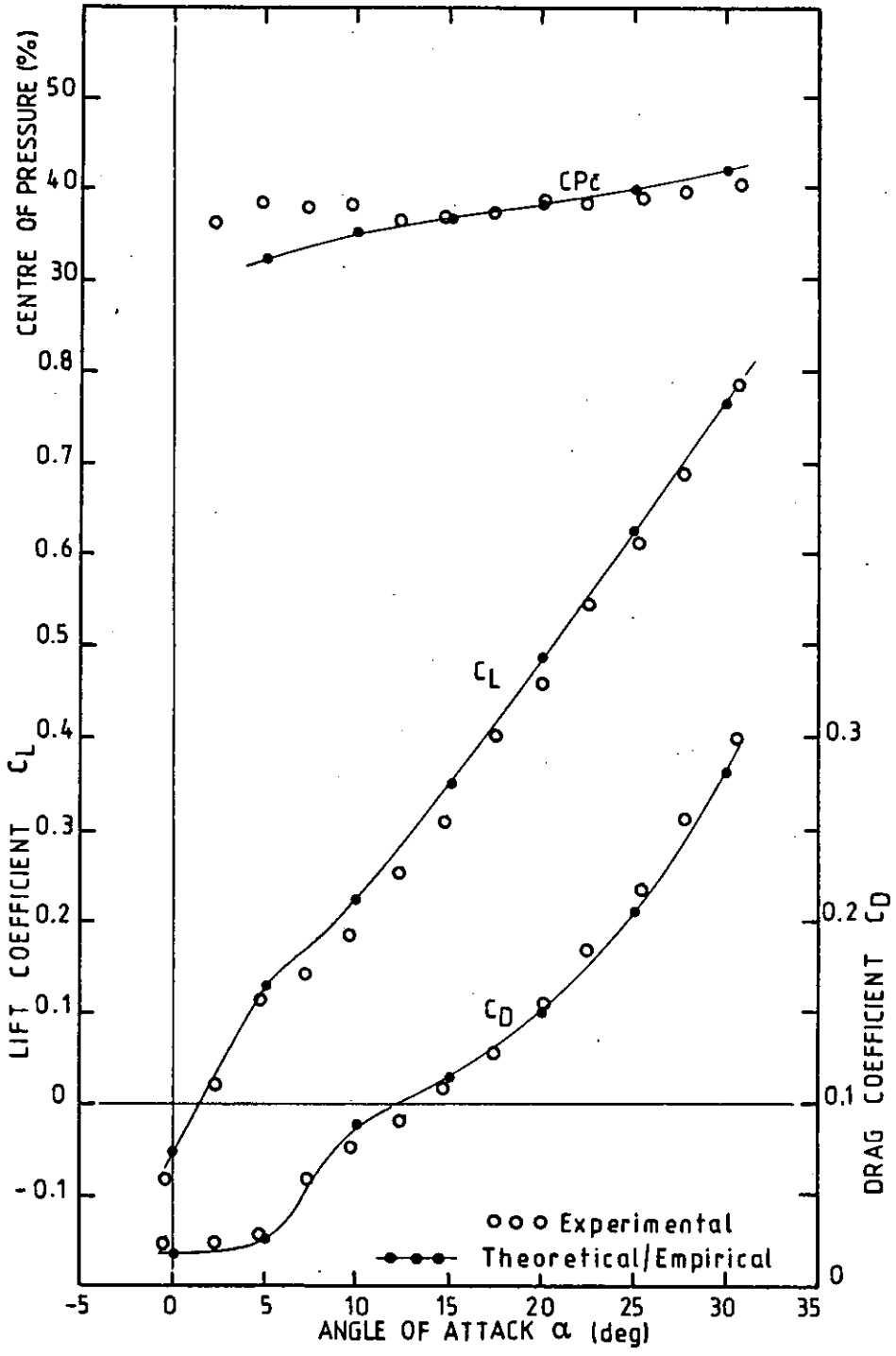

(a) Skeg Angle $\beta = -10.25°$; Taper Ratio = 0.60

Fig. 20 PREDICTIONS BY THEORETICAL / EMPIRICAL ANALYSIS

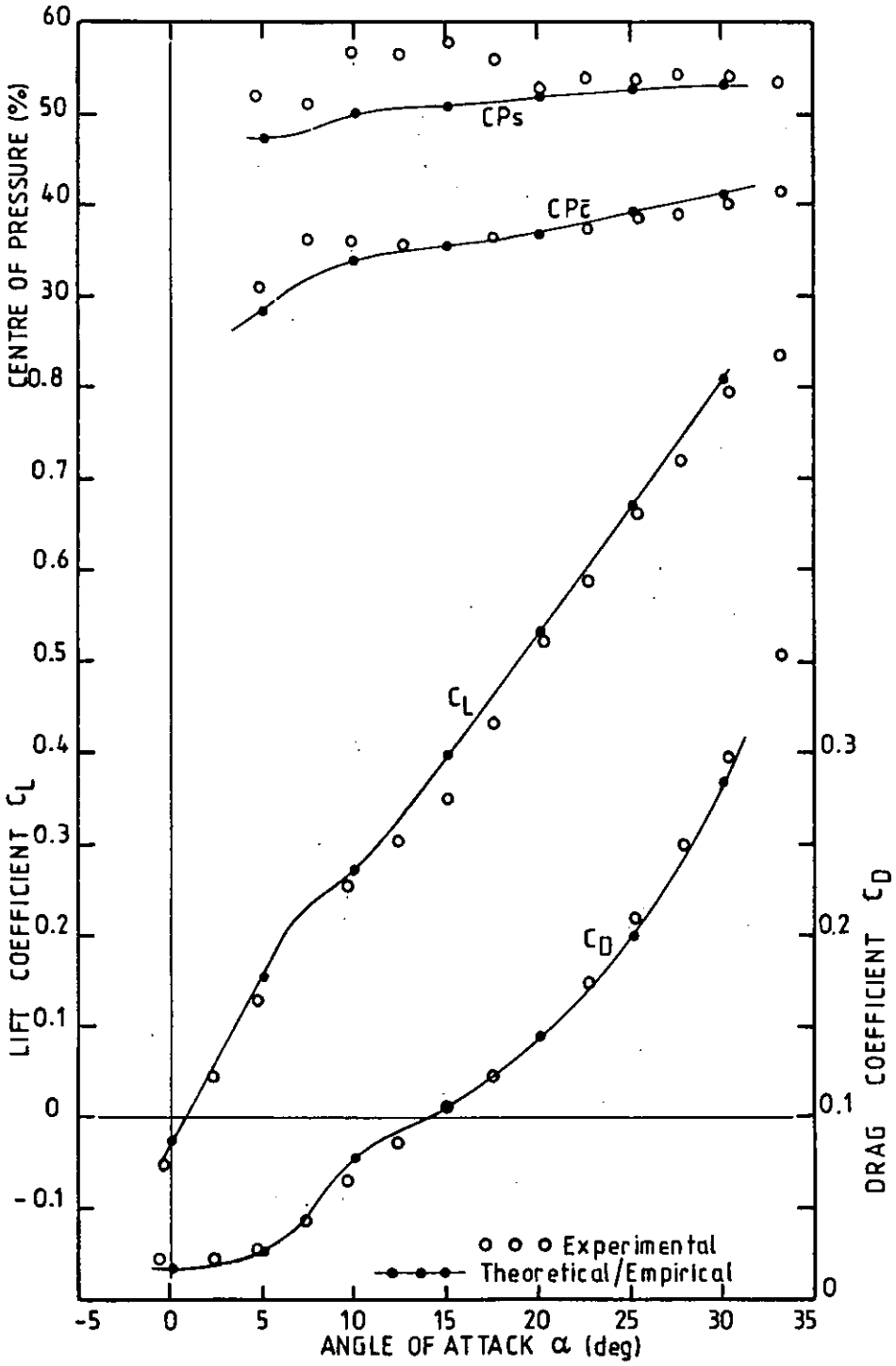

(b) Skeg Angle $\beta = -5.25°$; Taper Ratio=0.60

Fig. 20 (continued)

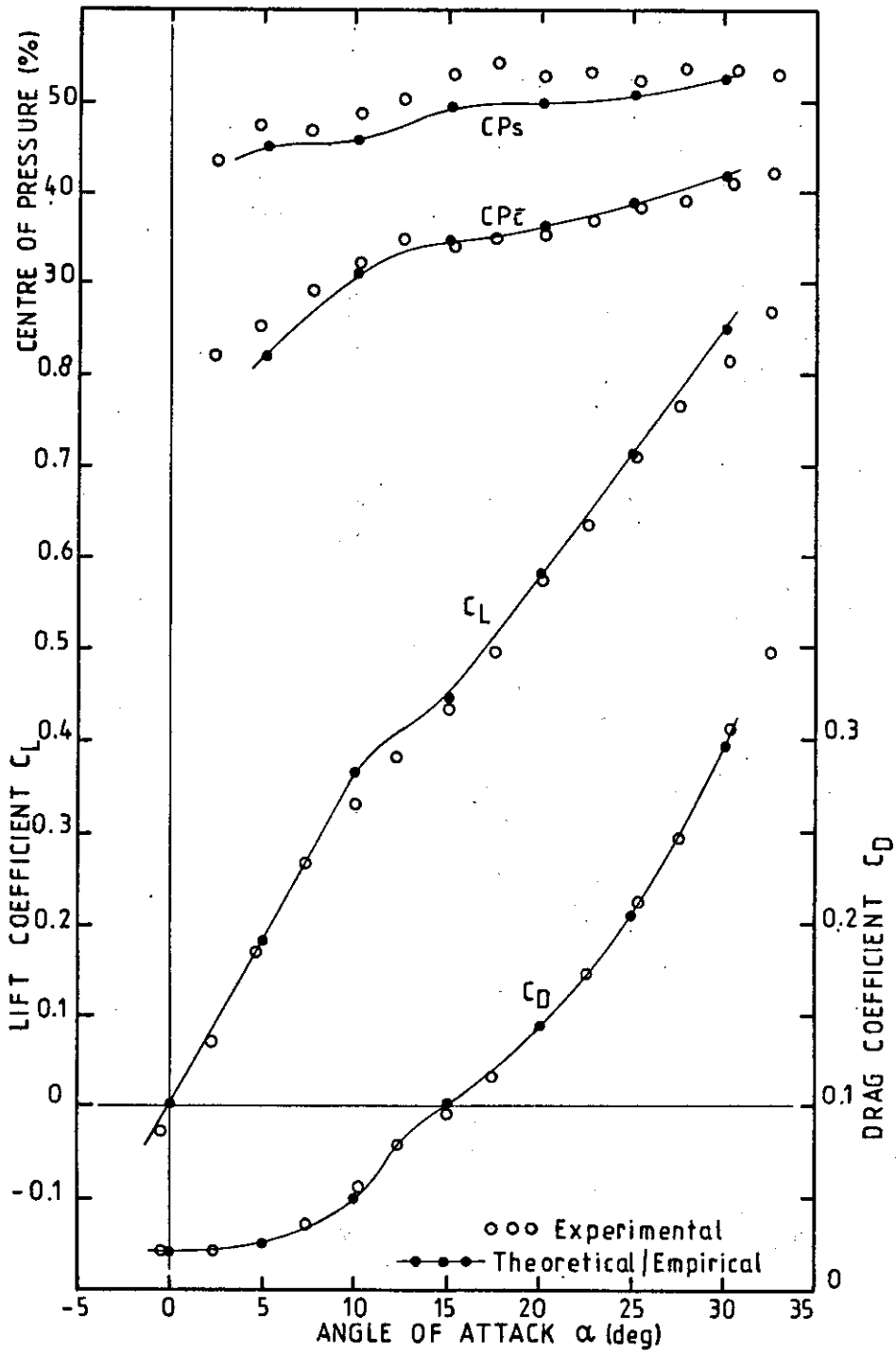

(c) Skeg Angle $\beta = -0.25°$; Taper Ratio=0.60

Fig. 20 (continued)

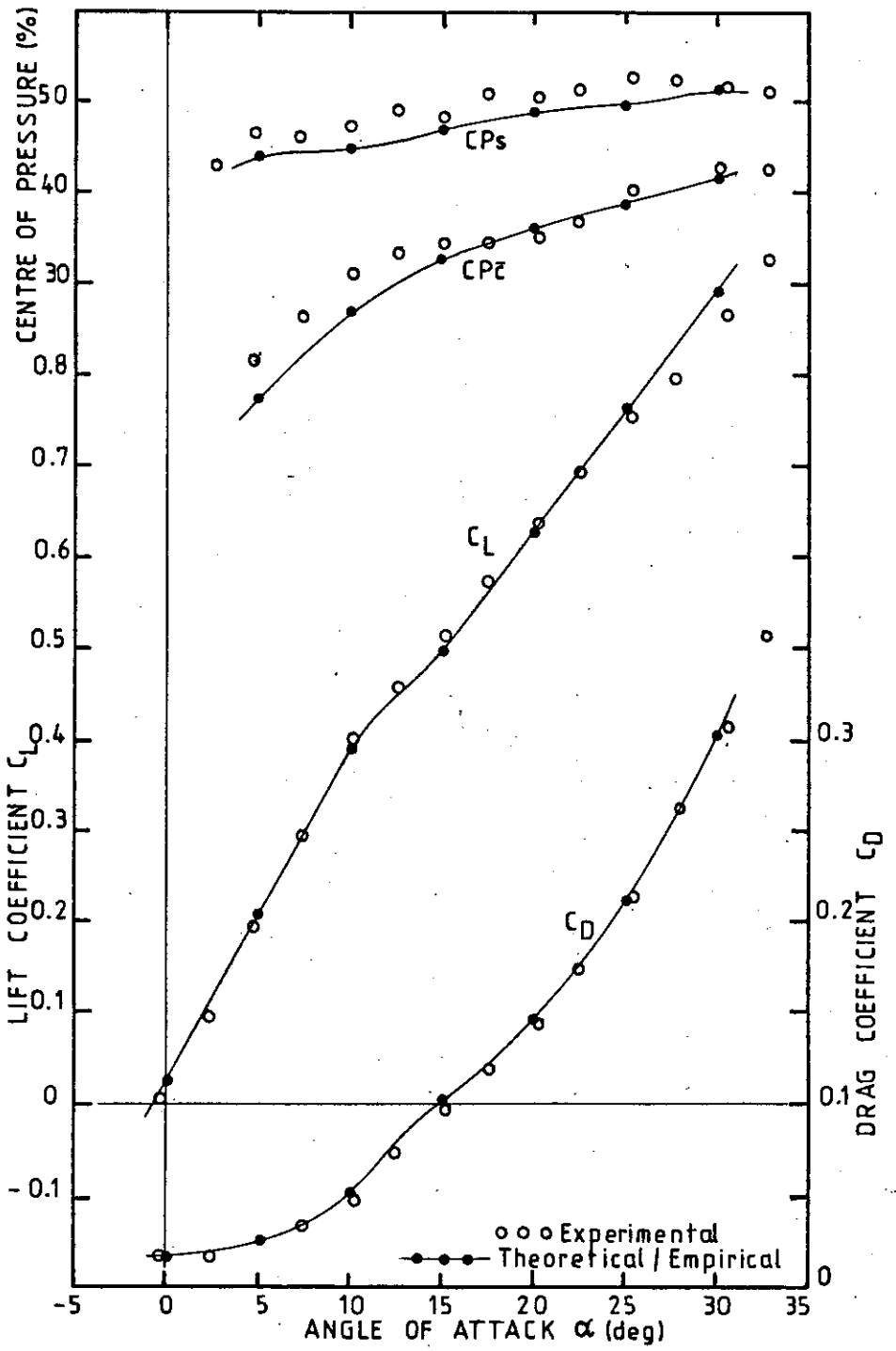

(d) Skeg Angle $\beta = +4.75°$; Taper Ratio=0.60

Fig. 20 (continued)

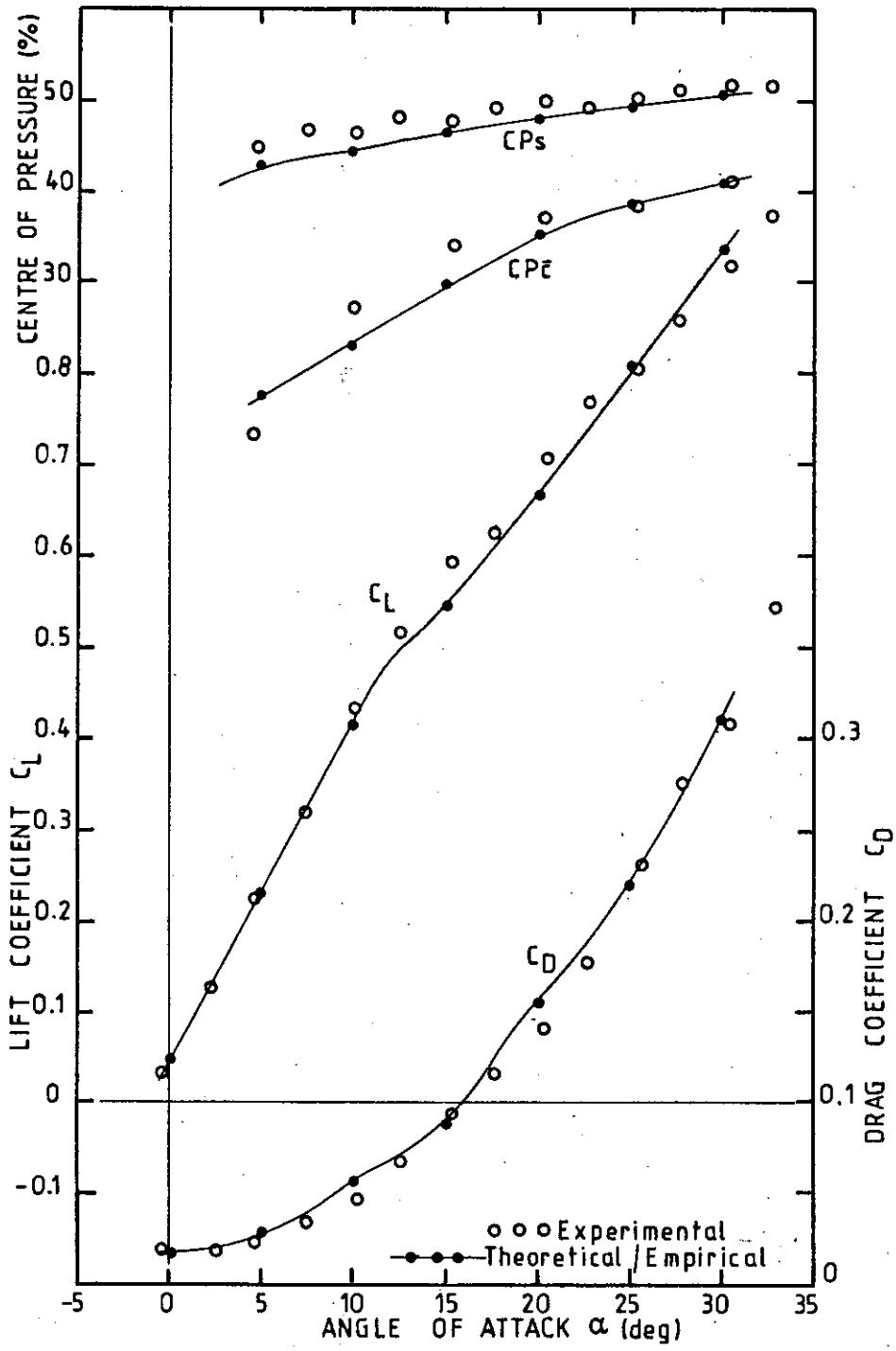

(e) Skeg Angle $\beta = +9.75°$; Taper Ratio=0.60

Fig. 20 (continued)

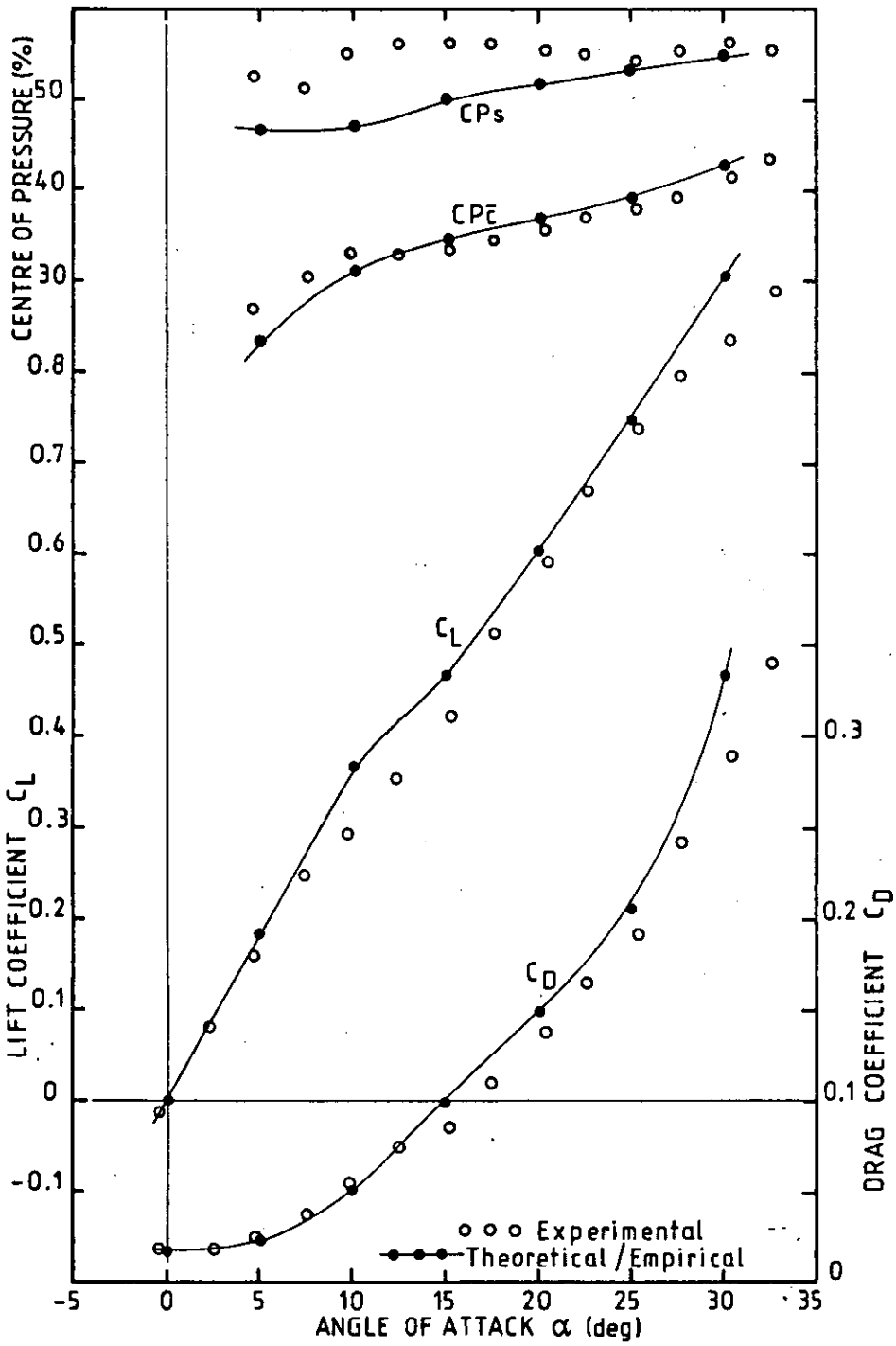

(a) Skeg Angle $\beta = -0.25°$; Taper Ratio=0.80

Fig. 21 PREDICTIONS BY THEORETICAL / EMPIRICAL ANALYSIS

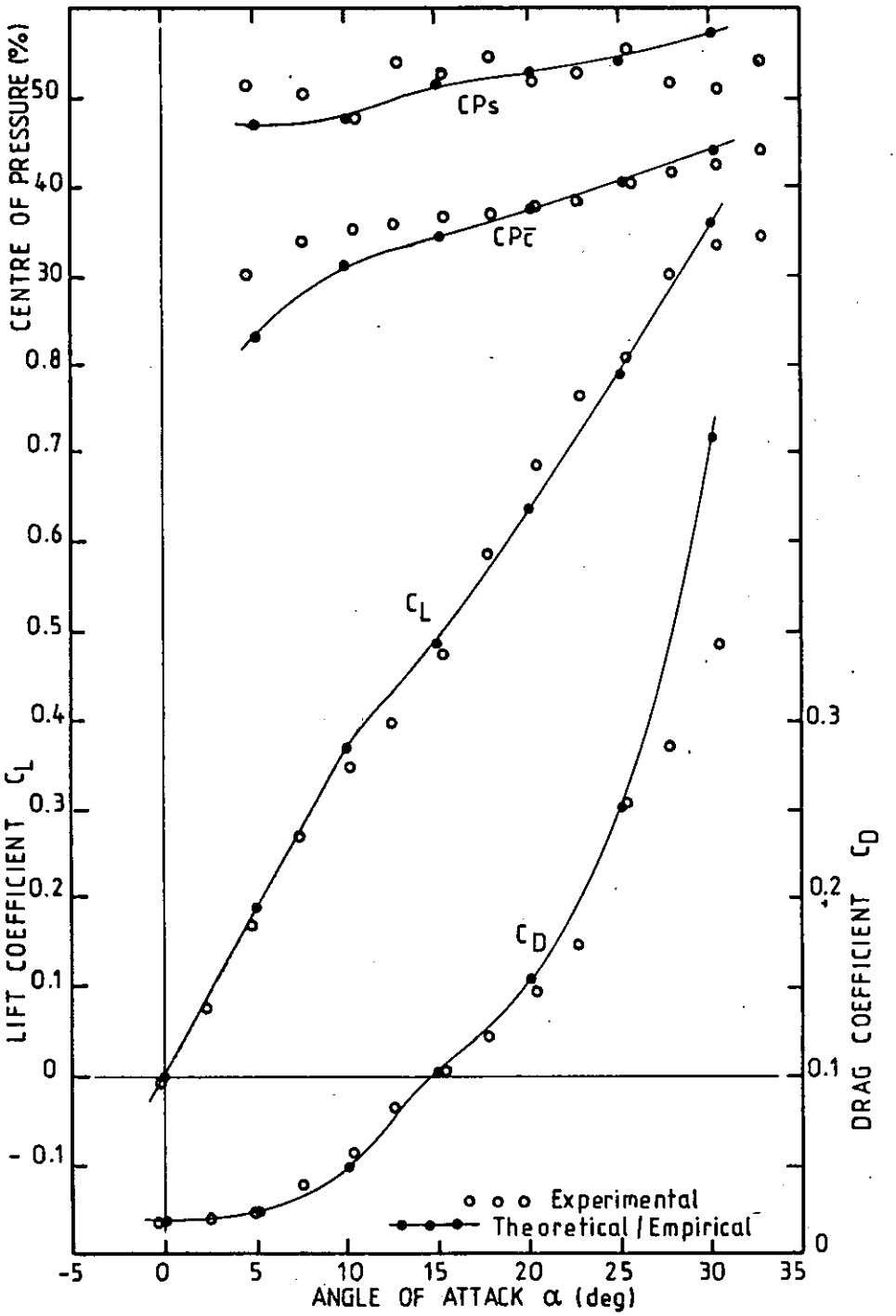

(b) Skeg Angle $\beta = -0.25°$; Taper Ratio=1.00

Fig. 21 (continued)

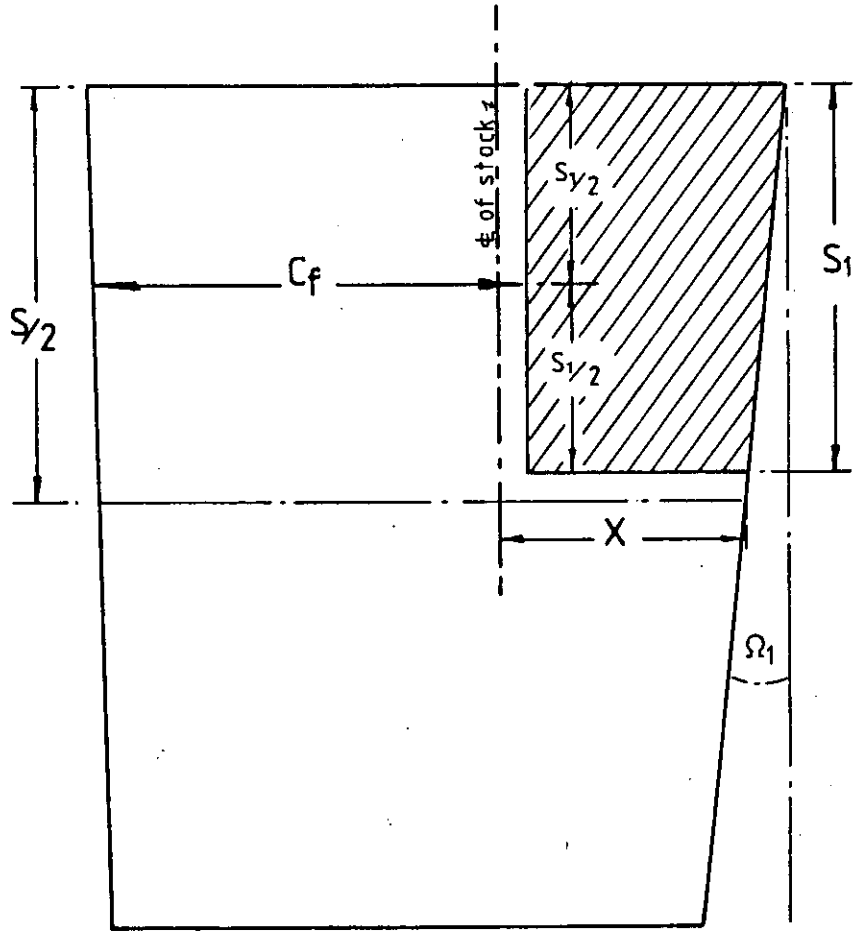

Fig. 22 SKEG DETAILS FEATURED IN PARAMETRIC STUDY

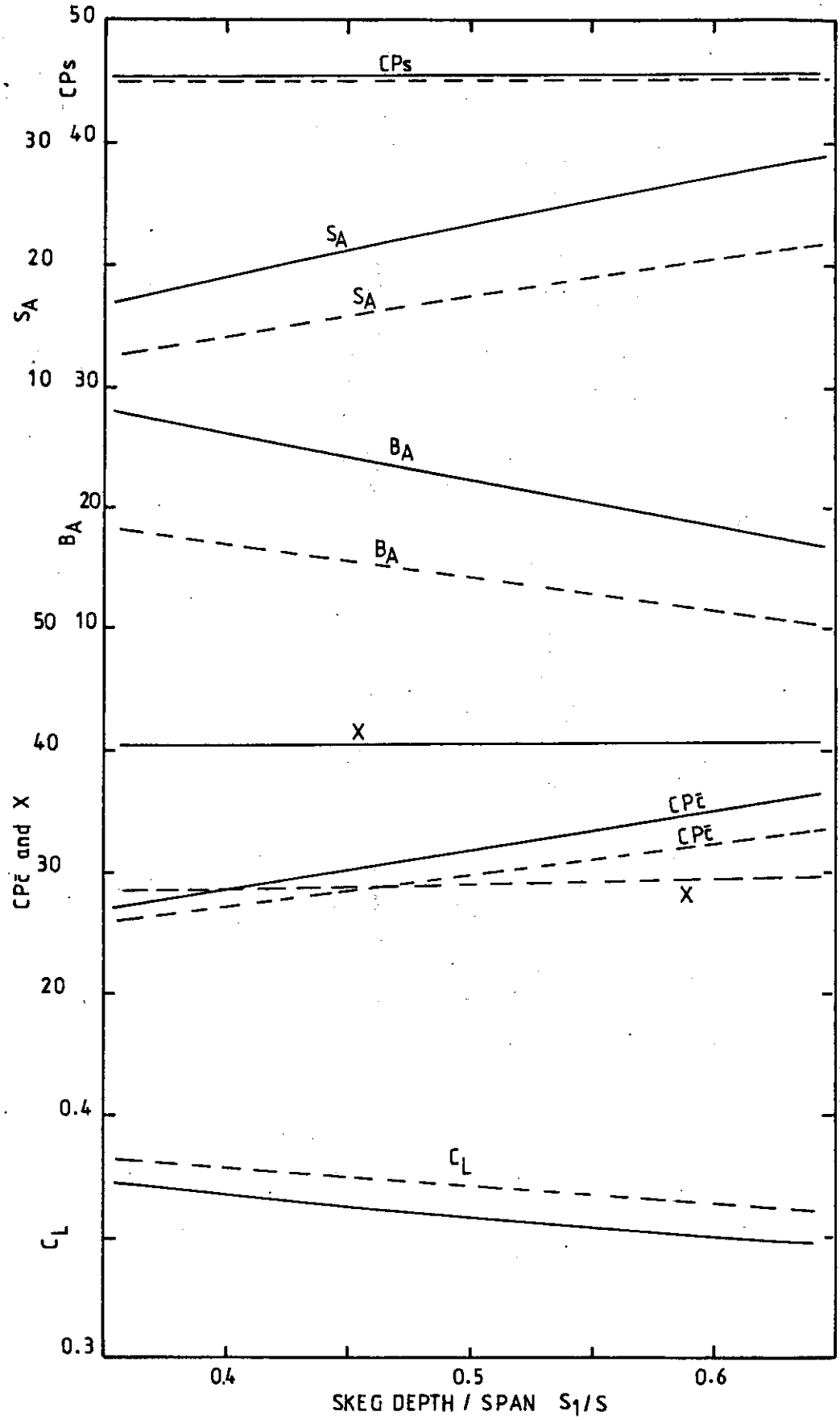

(a) $\alpha = 10°$

Fig. 23 VARIATION IN SKEG DEPTH and MOVABLE CHORD (Sweep constant)

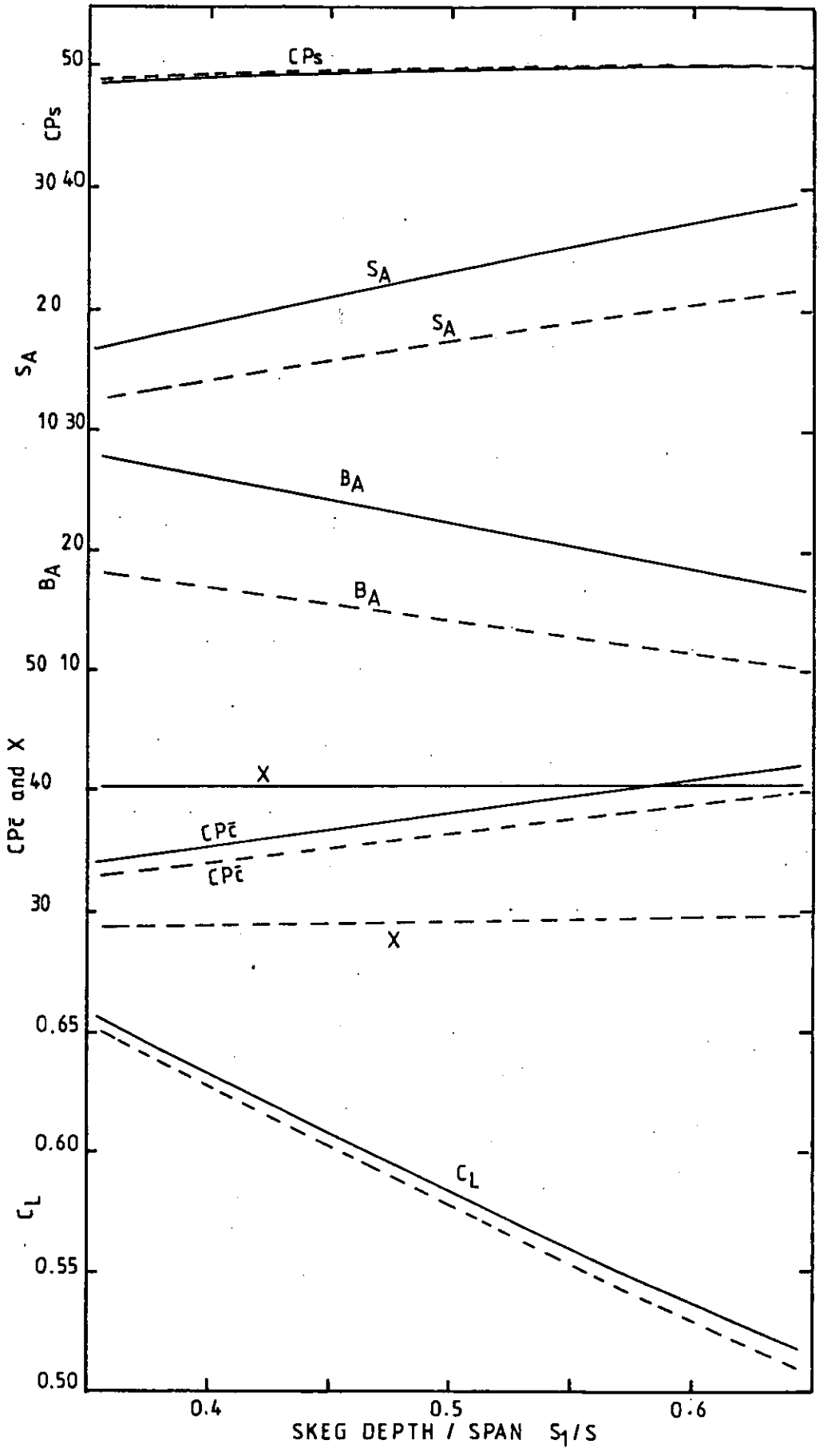

AR = 3; T = 0.6; $\Omega_1 = 0.153$; $\beta = 0°$

——— $C_f/c = 0.65$
- - - - - $C_f/c = 0.75$

(b) $\alpha = 20°$

Fig. 23 (continued)

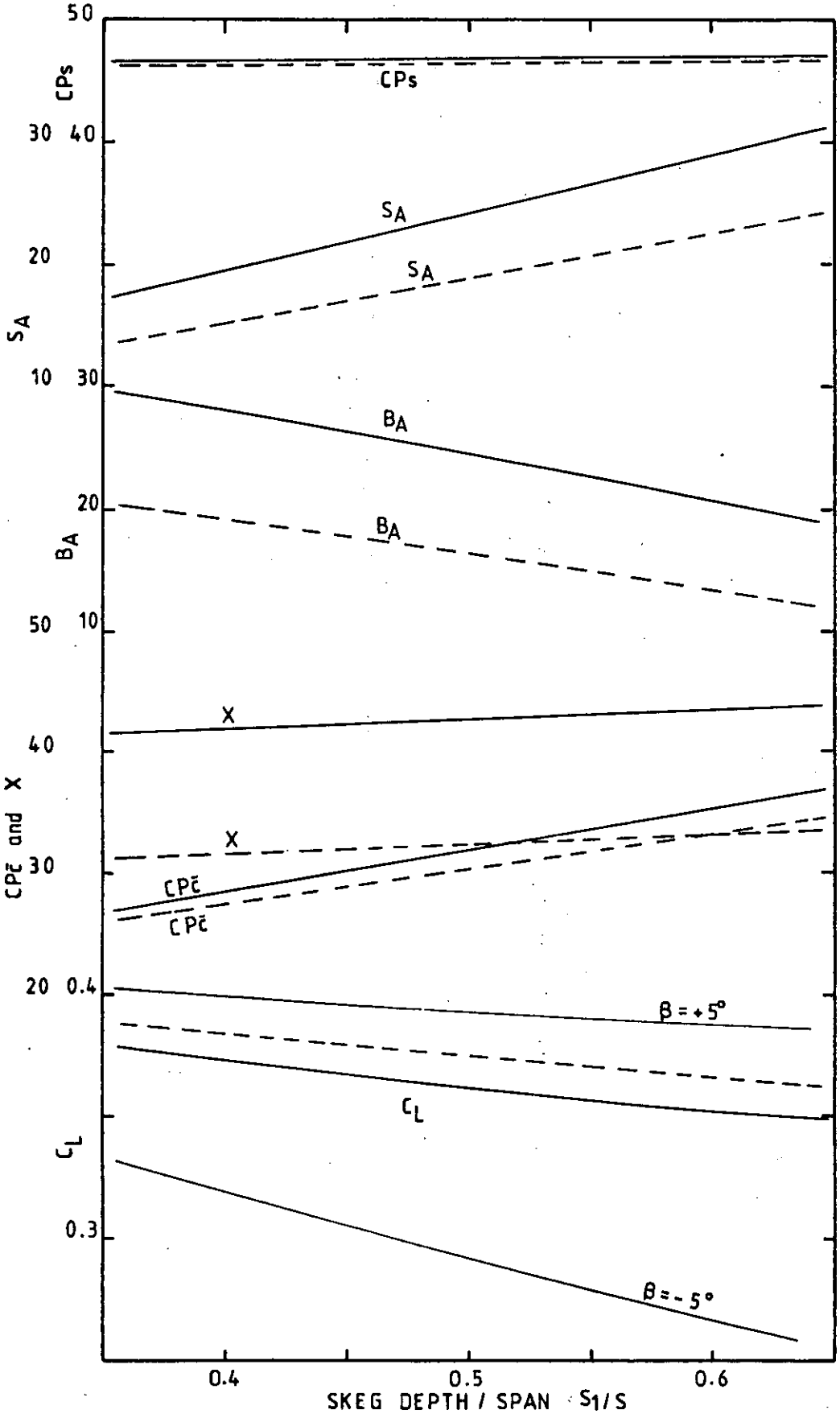

AR = 3; T = 0.8; Ω_1 = 0.153; β = 0°

——— C_f/c = 0.60

- - - - - C_f/c = 0.70

(a) $\alpha = 10°$

Fig. 24 VARIATION IN SKEG DEPTH and MOVABLE CHORD (Sweep constant)

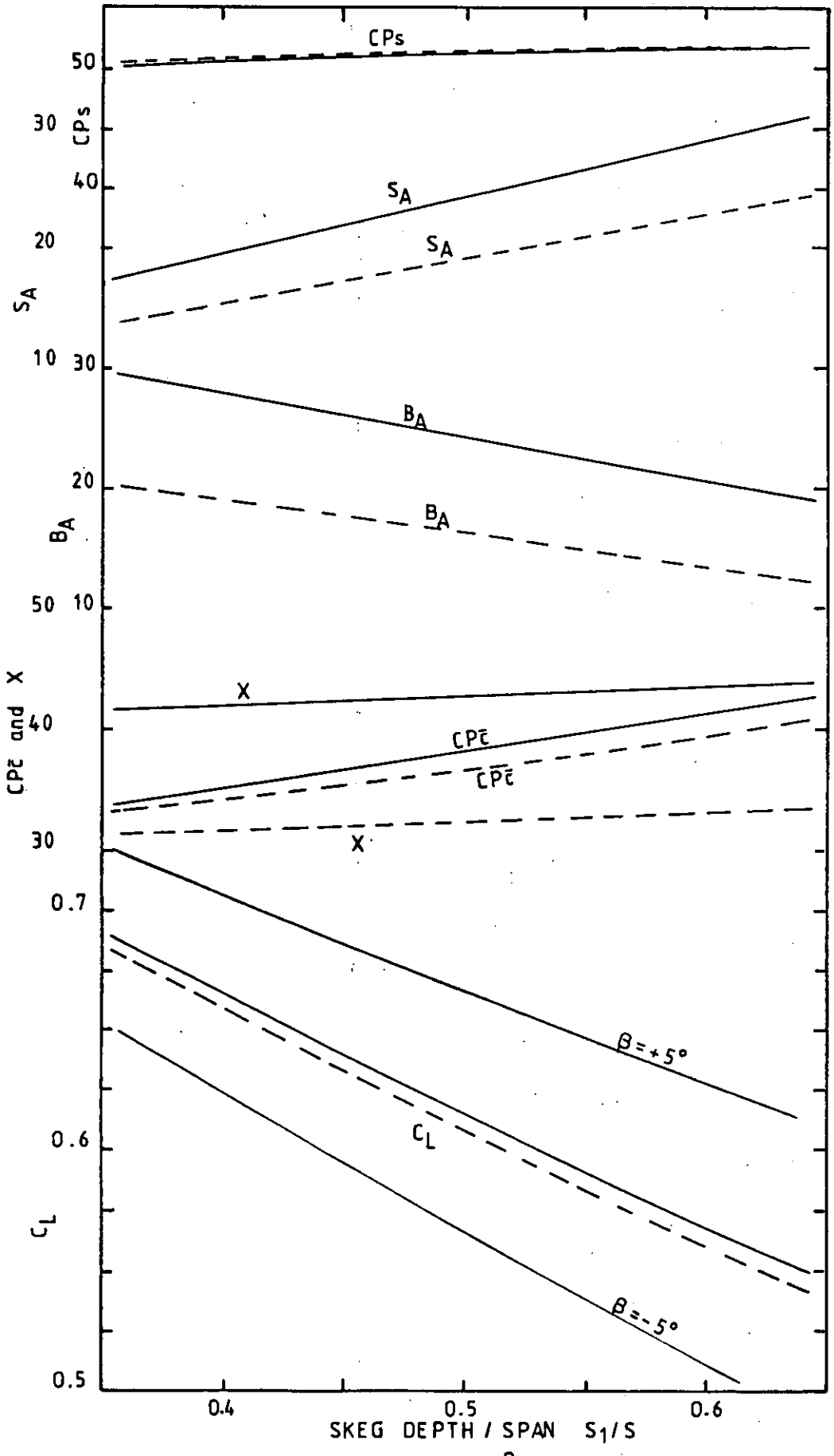

(b) $\alpha = 20°$

Fig. 24 (continued)

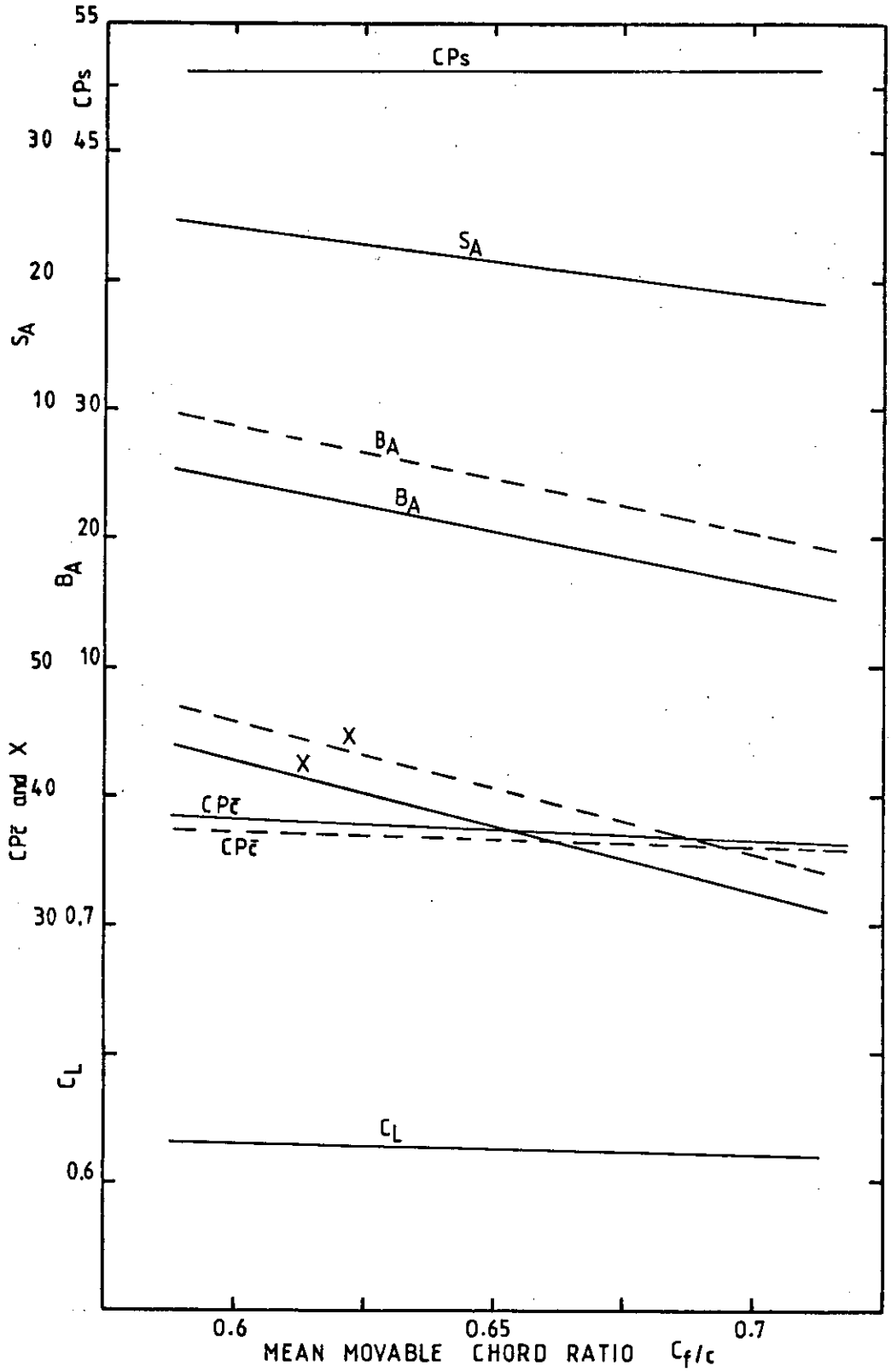

AR = 3; T = 0.8; $S_1/S = 0.5$; $\beta = 0°$

$\alpha = 20°$

——— $\Omega_1 = 0.153$

– – – $\Omega_1 = 0.070$

Fig. 25 VARIATION IN MOVABLE CHORD RATIO and SWEEP (Skeg depth constant)

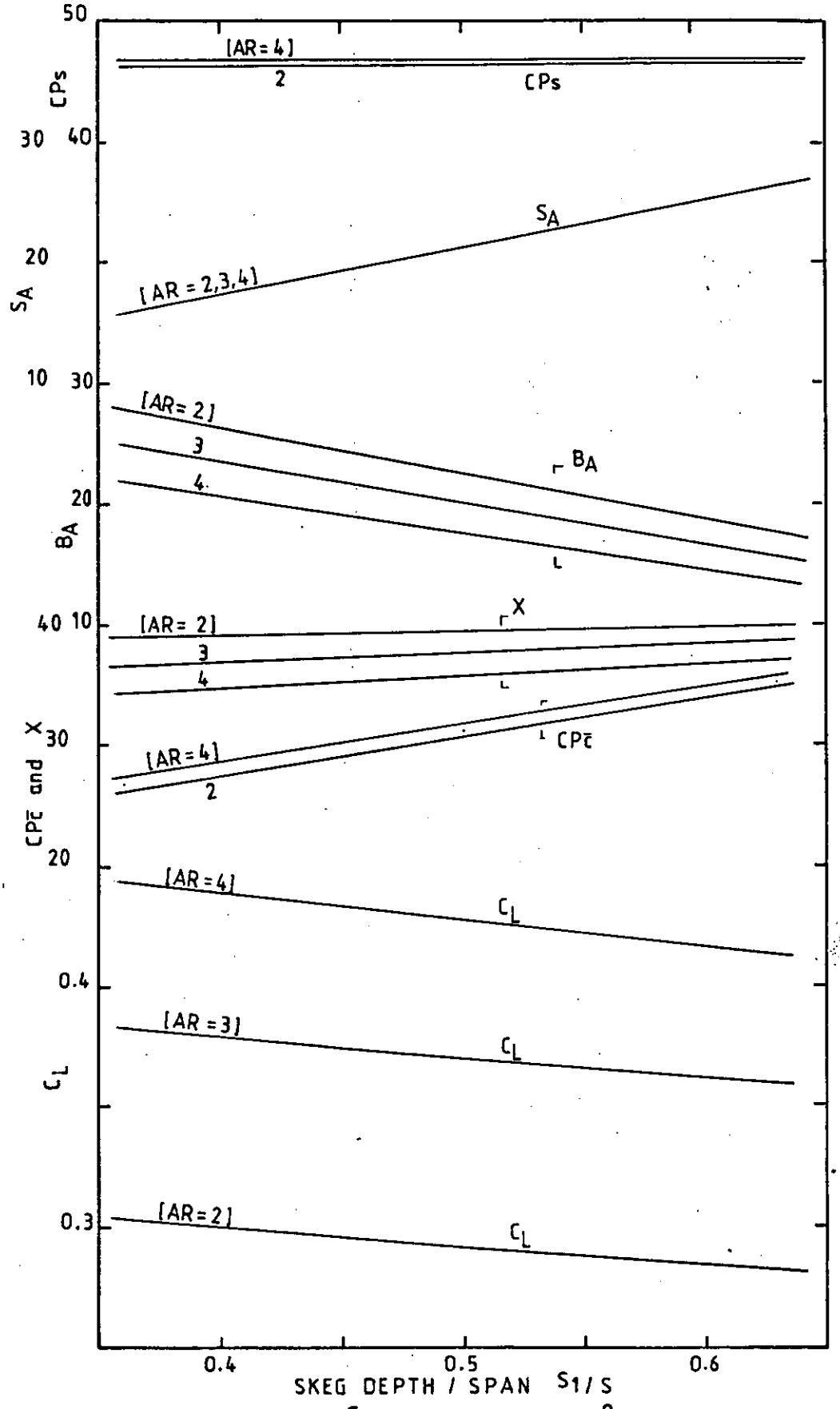

$T = 0.8$; $\Omega_1 = 0.153$; $C_f/c = 0.65$; $\beta = 0°$

$\alpha = 10°$

Fig. 26 VARIATION IN SKEG DEPTH and ASPECT RATIO